Report No. K-TRAN: KU-17-3 ▪ FINAL REPORT ▪ November 2019

Grouting Effects on Performance of Sliplined Steel Pipes

Jie Han, Ph.D., P.E., F.ASCE
Seyed Mustapha Rahmaninezhad, Ph.D.
Mahdi Al-Naddaf
Robert L. Parsons, Ph.D., P.E.
Saif Jawad
Hao Liu

The University of Kansas

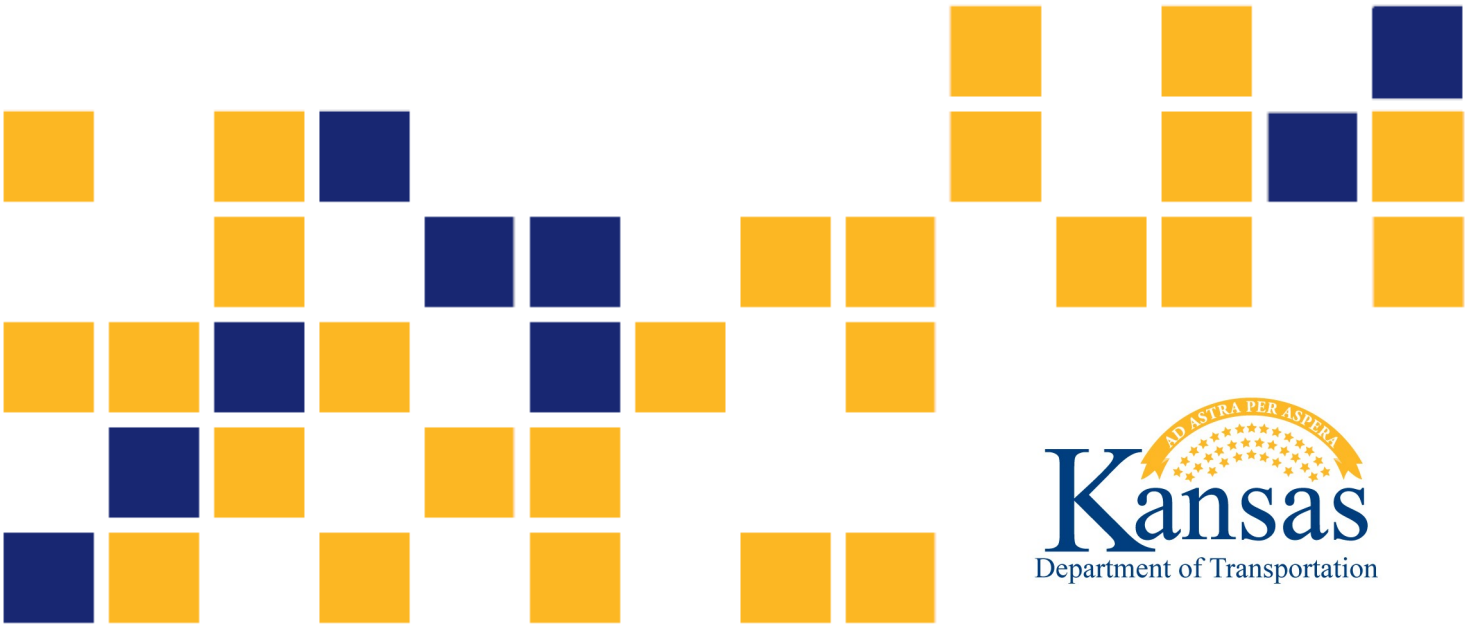

Kansas
Department of Transportation

1 Report No. K-TRAN: KU-17-3	**2 Government Accession No.**	**3 Recipient Catalog No.**
4 Title and Subtitle Grouting Effects on Performance of Sliplined Steel Pipes		**5 Report Date** November 2019 **6 Performing Organization Code**
7 Author(s) Jie Han, Ph.D., P.E., F.ASCE, Seyed Mustapha Rahmaninezhad, Ph.D., Mahdi Al-Naddaf, Robert L. Parsons, Ph.D., P.E., Saif Jawad, Hao Liu		**8 Performing Organization Report No.**
9 Performing Organization Name and Address The University of Kansas Department of Civil, Environmental & Architectural Engineering 1530 West 15th St Lawrence, Kansas 66045-7609		**10 Work Unit No. (TRAIS)** **11 Contract or Grant No.** C2095
12 Sponsoring Agency Name and Address Kansas Department of Transportation Bureau of Research 2300 SW Van Buren Topeka, Kansas 66611-1195		**13 Type of Report and Period Covered** Final Report September 2016–April 2019 **14 Sponsoring Agency Code** RE-0716-01
15 Supplementary Notes For more information write to address in block 9.		

16 Abstract

Culverts and pipes installed under roadways several decades ago are reaching the end of their service life. Excavation and replacement of these buried structures will cause disruption to their service and require significant funding. Trenchless methods (e.g., sliplining) have been increasingly used to rehabilitate deteriorated buried structures (e.g., corroded steel pipes). Sliplining involves placement of a new pipe liner inside an existing deteriorated pipe and filling of grout between their space. The objective of this study was to evaluate the effect of sliplining on the behavior of corrugated steel pipes with different degrees of corrosion under loading.

In this study, parallel-plate loading tests were carried out to evaluate the effect of sliplining on the behavior of corrugated steel pipes with different degrees of corrosion (0%, 50%, and 90%) in air. The corrosion in each steel pipe was simulated by cutting out steel segments along the invert of the pipe. A low-strength, normal density grout was used to fill the space between the steel pipe and the liner. The unlined and sliplined pipes were tested for their load-carrying capacities, stiffness, vertical and horizontal diameter changes, and average strains and curvatures. The test results show that prior to sliplining, the steel pipe with 90% cutout behaved stiffer than that with 50% cutout at a higher applied load. After sliplining, however, the steel pipe with 50% cutout had higher stiffness than the pipe with 90% cutout. Sliplining increased the load-carrying capacity and stiffness of the pipe. The location of the liner relative to the existing pipe wall had a minor effect on the behavior of the sliplined steel pipes. This study investigated the effect of sliplining on the performance of a highly corroded corrugated steel pipe. An existing pipe placed under an asphalt pavement was investigated. A low-viscosity grout was used to fill the space between the steel pipe and the liner. A series of truck loading and plate loading tests were conducted before and after sliplining of the steel pipe to determine: (1) load-carrying behavior and stiffness; (2) vertical and horizontal diameter changes; (3) average strain and curvature of pipes; and (4) settlement of the pavement surface. Moreover, deformations, strains, and curvatures around the circumference of the liner were monitored during sliplining and service time. The sliplined corroded steel pipe had considerably higher stiffness than the corroded pipe. For the truck loading test conducted at 28 days after grouting, the sliplining reduced the vertical diameter changes of the corroded steel pipe by about 81%. For the field plate loading tests, the sliplining for 7 and 28 days reduced the settlement of the pavement by 6% and 30%, respectively, as compared with that before sliplining.

During the experimental model study, six footing loading tests were conducted on the unlined and sliplined buried steel corrugated pipes with different degrees of corrosion in soil. The reduced-scale models were constructed in a test box under a plane-strain condition and tested under static footing loads. A low-viscosity grout was used to fill the space between the steel pipe and the liner. After the footing loading tests were conducted, the sliplined steel pipes were exhumed from the box. Then, a series of parallel plate loading tests was carried out on the exhumed rehabilitated pipes using a universal testing machine. The results show that the measured earth pressures induced by footing loading above the crown of the unlined pipe with 0% cutout were higher than those with 50% and 90% cutout. However, the degree of corrosion did not have significant effect on the earth pressures induced by footing loading above the crown of the sliplined pipes.

17 Key Words Sliplining, Corrugated Pipe, Deterioration, Grouting		**18 Distribution Statement** No restrictions. This document is available to the public through the National Technical Information Service www.ntis.gov.	
19 Security Classification (of this report) Unclassified	**20 Security Classification (of this page)** Unclassified	**21 No. of pages** 88	**22 Price**

Form DOT F 1700.7 (8-72)

This page intentionally left blank.

Grouting Effects on Performance of Sliplined Steel Pipes

Final Report

Prepared by

Jie Han, Ph.D., P.E., F.ASCE
Seyed Mustapha Rahmaninezhad, Ph.D.
Mahdi Al-Naddaf
Robert L. Parsons, Ph.D., P.E.
Saif Jawad
Hao Liu

The University of Kansas

A Report on Research Sponsored by

THE KANSAS DEPARTMENT OF TRANSPORTATION
TOPEKA, KANSAS

and

THE UNIVERSITY OF KANSAS
LAWRENCE, KANSAS

November 2019

PREFACE

The Kansas Department of Transportation's (KDOT) Kansas Transportation Research and New-Developments (K-TRAN) Research Program funded this research project. It is an ongoing, cooperative and comprehensive research program addressing transportation needs of the state of Kansas utilizing academic and research resources from KDOT, Kansas State University and the University of Kansas. Transportation professionals in KDOT and the universities jointly develop the projects included in the research program.

NOTICE

The authors and the state of Kansas do not endorse products or manufacturers. Trade and manufacturers names appear herein solely because they are considered essential to the object of this report.

This information is available in alternative accessible formats. To obtain an alternative format, contact the Office of Public Affairs, Kansas Department of Transportation, 700 SW Harrison, 2nd Floor – West Wing, Topeka, Kansas 66603-3745 or phone (785) 296-3585 (Voice) (TDD).

DISCLAIMER

The contents of this report reflect the views of the authors who are responsible for the facts and accuracy of the data presented herein. The contents do not necessarily reflect the views or the policies of the state of Kansas. This report does not constitute a standard, specification or regulation.

Abstract

Culverts and pipes installed under roadways several decades ago are reaching the end of their service life. Excavation and replacement of these buried structures will cause disruption to their service and require significant funding. Trenchless methods (e.g., sliplining) have been increasingly used to rehabilitate deteriorated buried structures (e.g., corroded steel pipes). Sliplining involves placement of a new pipe liner inside an existing deteriorated pipe and filling of grout between their space. The objective of this study was to evaluate the effect of sliplining on the behavior of corrugated steel pipes with different degrees of corrosion under loading.

In this study, parallel-plate loading tests were carried out to evaluate the effect of sliplining on the behavior of corrugated steel pipes with different degrees of corrosion (0%, 50%, and 90%) in air. The corrosion in each steel pipe was simulated by cutting out steel segments along the invert of the pipe. A low-strength, normal density grout was used to fill the space between the steel pipe and the liner. The unlined and sliplined pipes were tested for their load-carrying capacities, stiffness, vertical and horizontal diameter changes, and average strains and curvatures. The test results show that prior to sliplining, the steel pipe with 90% cutout behaved stiffer than that with 50% cutout at a higher applied load. After sliplining, however, the steel pipe with 50% cutout had higher stiffness than the pipe with 90% cutout. Sliplining increased the load-carrying capacity and stiffness of the pipe. The location of the liner relative to the existing pipe wall had a minor effect on the behavior of the sliplined steel pipes.

This study investigated the effect of sliplining on the performance of a highly corroded corrugated steel pipe. An existing pipe placed under an asphalt pavement was investigated. A low-viscosity grout was used to fill the space between the steel pipe and the liner. A series of truck loading and plate loading tests were conducted before and after sliplining of the steel pipe to determine: (1) load-carrying behavior and stiffness; (2) vertical and horizontal diameter changes; (3) average strain and curvature of pipes; and (4) settlement of the pavement surface. Moreover, deformations, strains, and curvatures around the circumference of the liner were monitored during sliplining and service time. The sliplined corroded steel pipe had considerably higher stiffness than the corroded pipe. For the truck loading test conducted at 28 days after grouting, the sliplining

reduced the vertical diameter changes of the corroded steel pipe by about 81%. For the field plate loading tests, the sliplining for 7 and 28 days reduced the settlement of the pavement by 6% and 30%, respectively, as compared with that before sliplining.

During the experimental model study, six footing loading tests were conducted on the unlined and sliplined buried steel corrugated pipes with different degrees of corrosion in soil. The reduced-scale models were constructed in a test box under a plane-strain condition and tested under static footing loads. A low-viscosity grout was used to fill the space between the steel pipe and the liner. After the footing loading tests were conducted, the sliplined steel pipes were exhumed from the box. Then, a series of parallel plate loading tests was carried out on the exhumed rehabilitated pipes using a universal testing machine. The results show that the measured earth pressures induced by footing loading above the crown of the unlined pipe with 0% cutout were higher than those with 50% and 90% cutout. However, the degree of corrosion did not have significant effect on the earth pressures induced by footing loading above the crown of the sliplined pipes.

Acknowledgements

This research project was financially sponsored by the Kansas Department of Transportation (KDOT). Mr. Dave Meggers, Chief of the KDOT Bureau of Research, was the project monitor. Contech Engineered Solutions LLC provided the steel pipes used in the experimental tests and Mr. Bill Gonsalez, the Territory Sales Representative, provided great assistance in this study. The Public Works Department of Douglas County, Kansas; Mr. Keith A. Browning, Director/County Engineer; Ms. Agamani Sen, Engineering Manager; Mr. Doug Stephens, Operations Division Manager; Mr. Rod Heard, Road and Bridge Maintenance Supervisor; and Mr. Reggie Demby provided great assistance in the field study. The Laboratory Manager, Mr. David Woody, and technician, Mr. Kent Dye, of the Department of Civil, Environmental, and Architectural Engineering (CEAE) at the University of Kansas (KU) provided their technical support. Furthermore, the visiting scholars, Ms. Fengjuan Tao and Dr. Yuan Cheng, from the KU CEAE Department provided assistance in the laboratory testing.

Table of Contents

List of Tables

List of Figures

Chapter 1: Introduction

1.1 Background

Some buried structures, such as culverts and pipes, installed under roadways for several decades are going to reach the end of their service life (Ballinger and Drake, 1995; Mai, 2013; Mai et al. 2013; Smith et al., 2015; Simpson et al., 2015; Simpson et al., 2017; Al-Naddaf et al. 2018; Han et al. 2018). They are vulnerable to crushing due to surface loading if shallowly buried (Acharya et al., 2014). Replacement of these buried structures requires excavation, removal, placement, and compaction (Wang et al., 2015) that will cause disruption to roadways and require significant funding. Therefore, most of these buried structures cannot be replaced efficiently (Smith et al., 2015; Simpson et al., 2015). Trenchless rehabilitation methods have been increasingly used to reduce overall project cost and disruption to service as compared with the excavation and replacement method. Sliplining is the most common trenchless rehabilitation method used for corrugated steel pipes, where a new pipe liner of smaller diameter is placed inside an existing deteriorated pipe and grout is used to fill the space between them (Smith et al., 2015; Simpson et al., 2015). The commonly-used liners are plastic pipes made of high-density polyethylene (HDPE) or polyvinyl chloride (PVC) (Simpson et al., 2017). In general, sliplining can improve the structural and drainage capacity of deteriorated steel pipes (Smith et al., 2015, Mai, 2013).

Mai (2013) and Mai et al. (2013) evaluated the stability of two steel pipes with different degrees of corrosion, which were exhumed from the field. They investigated the behavior of the pipes using the parallel-plate loading test on one deteriorated corrugated steel pipe and surface loading tests on buried pipes. They observed localized bending in the crown and buckling of the remaining steel in the corroded region at failure. Simpson et al. (2015) conducted a series of surface loading tests on buried deteriorated corrugated steel pipes at two different burial depths before and after sliplining rehabilitation to evaluate the benefit of the liner and grout. They found that the rehabilitated pipe was considerably stiffer and the diameter changes under surface loading were reduced by more than 90% as compared with the un-rehabilitated pipe. Smith et al. (2015) carried out a series of the parallel-plate loading tests to evaluate the effect of grout strength on the load-carrying capacity and stiffness of slip-lined corrugated steel pipes. In their study, liners were placed

at the center of the existing steel pipes. They found that the rehabilitated steel pipe with low-strength grout had increased the load-carrying capacity by more than three times as compared with the un-rehabilitated pipe. The use of high-strength grout resulted in an increase in the load-carrying capacity by more than 10 times as compared with the un-rehabilitated pipe. Regier (2015) conducted a series of the surface loading tests on buried deteriorated corrugated steel pipes to compare their behavior with intact pipes. Regier (2015) observed local buckling in the area of corrosion perforations and local bending across the crown of the pipes. Simpson et al. (2017) conducted an experimental study to evaluate the performance of two damaged reinforced concrete pipes in soil under surface loading before and after sliplining. They found that sliplining increased the stiffness of the pipes significantly and reduced the vertical diameter deformations by 87% to 93%.

1.2 Problem Statement

Although sliplining is a preferred rehabilitation approach, limited studies have been conducted so far on: (1) effect of degree of corrosion on the behavior of sliplined pipes; (2) effect of the grout area and strength on the behavior of sliplined pipes; (3) field evaluation of sliplining rehabilitation; and (4) effect of the sliplining rehabilitation on the surrounding soil (especially in the bedding soil) of the corroded pipes.

1.3 Research Objectives

The objectives of this research were: (1) to examine the effect of degree of corrosion on the behavior of unlined and sliplined corrugated steel pipes; (2) to evaluate the effect of the grout area and strength on the behavior of sliplined corroded corrugated steel pipes; and (3) to evaluate the effect of sliplining rehabilitation on field performance of corroded corrugated steel pipes.

1.4 Research Methodology

The methodology adopted in this research included: (1) a comprehensive literature review of the research in this application; (2) a series of parallel-plate loading tests on unlined and sliplined corrugated steel pipes in air with different degrees of corrosion and different types of grout using a universal testing machine; (3) a series of surface footing loading tests on unlined and sliplined

corrugated steel pipes in soil with different degrees of corrosion using a geotechnical testing box; and (4) a field evaluation of the performance of a highly corroded corrugated steel pipe, before and after sliplining, using truck loading and plate loading tests. Laboratory and field evaluations yielded the following results: (1) load-carrying behavior and stiffness of steel pipes; (2) diameter changes of steel pipes and liners; (3) average strains and curvatures of steel pipes and liners; and (4) settlement of the road surface.

1.5 Organization of Report

This report is divided into six chapters. Chapter 1 describes the background, problem statement, research objectives, and research methodology. Chapter 2 presents a literature review on relevant topics of this research. The effect of sliplining rehabilitation on the behavior of corroded corrugated steel pipes under parallel-plate loading in air is presented in Chapter 3. Chapter 4 presents the effect of sliplining on the behavior of a highly corroded corrugated steel pipe that was placed at a shallow depth under an asphalt pavement in the field. Chapter 5 presents the effect of sliplining on the behavior of buried corroded corrugated steel pipes in sand under footing loading in a geotechnical test box. Chapter 6 presents the conclusions and recommendations drawn from this study.

Chapter 2: Literature Review

This chapter presents a literature review on relevant topics of the research, including the Culvert Repair Practices Manual (Ballinger & Drake, 1995) of the Federal Highway Administration (FHWA) about sliplining and the publications of other previous studies on sliplining.

2.1 FHWA Culvert Repair Practices Manual

Based on the FHWA Culvert Repair Practices Manual (Ballinger and Drake, 1995), sliplining is one of the effective ways to restore a culvert to a functional condition and includes the process of lining an existing culvert with either a conventional or new type of prefabricated culvert product. Any type of culvert can be sliplined with another type of culvert. However, proper selection of the most relevant material depends upon several factors, including: (1) type and size of the existing culvert; (2) site-specific conditions; (3) effluent characteristics; (4) design life requirements; (5) service life assigned; (6) economic factors; and (7) expected maintenance.

Depending on materials and methods, sliplining may be able to restore the structural strength of deteriorated culverts and to reduce the loss in hydraulic conductivity. Moreover, sliplining may eliminate the environmental effects that led to the deterioration of the existing culvert (e.g., the influence of acid mine runoff or caustic water) by selecting a proper lining material that is resistant to such conditions. Though sliplining may reduce the internal cross-sectional area of the existing culvert, some liners having a lower roughness coefficient than that of the existing culvert can maintain or improve the hydraulic capacity. Even though a variety of methods may be employed to slipline a culvert, the following steps are commonly required for the sliplining process:

1. Control water draining through the culvert,
2. Clean and repair damaged areas in the existing culvert if necessary before sliplining,
3. Repair the embankment if necessary,
4. Provide a guideway on the culvert to facilitate grouting,
5. Place the liner in the culvert,

6. Grout the space between the existing culvert and the liner, and
7. Check to ensure complete grouting of annular space.

FHWA has allowed the use of different types of liners, e.g., corrugated metal pipe, precast concrete pipe, high-density polyethylene (HDPE) pipe, polyvinyl chloride (PVC) pipe, and fiberglass pipe, to line existing culverts. Moreover, a variety of grouting materials may be used to fill the space between the liner and the existing culvert. A portland cement-based mortar and a controlled low strength material (CLSM) are typically used as grout. FHWA noted that the grout may not be required to have the strength of structural concrete but rather it may only need the strength of well-compacted soil. A CLSM is usually a mix of cement, fly ash, fine sand, and water. Tables 2.1 and 2.2 provide the CLSM mix design and the fine aggregate gradation suggested by FHWA.

Table 2.1: CLSM mix design suggested by FHWA

Materials	Quantities	
	US units	SI units
Cement	100 lbs/yd^3	59 kg/m^3
Fly Ash	300 lbs/yd^3	178 kg/m^3
Fine Aggregate	2600 lbs/yd^3	1542 kg/m^3
Water (approximate)	70 gal	265 liter

Source: Ballinger and Drake (1995)

Table 2.2: Fine aggregate gradation suggested by FHWA

Sieve size	% passing
¾ inch	100
No. 200	0–10

Source: Ballinger and Drake (1995)

2.2 Mai et al. (2013)

Mai et al. (2013) compared the performance of two corroded corrugated metal (steel) pipes (CMP) during backfilling and under surface loading. The diameter and the intact wall thickness of CMPs were 1.8 m and 4.5 mm, respectively. The average degrees of corrosion along both sides of the invert of the extensively corroded CMP were 30% and 52%, and those for the lightly corroded CMP were 17% and 10%. The fill material was a well-graded sandy gravel, which is classified as A-1 by AASHTO (2009). The CMPs were backfilled with 0.6 and 0.9 m thick cover and loaded by a steel pad. Figure 2.1 shows the vertical and horizontal diameter changes of the corroded CMPs

during backfilling. During backfilling from the invert to the crown, the diameter changes of both CMPs were similar. However, these CMPs performed differently under the overburden pressure. The difference in the performance of the CMPs was due to their different stiffness values.

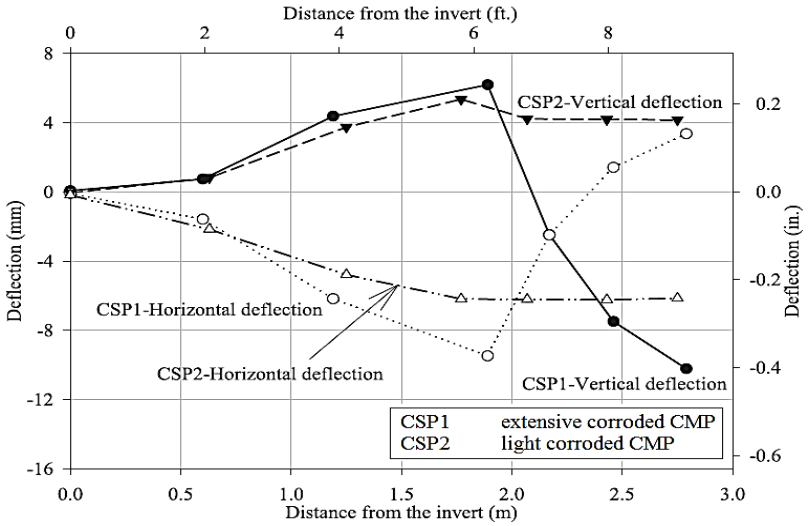

Figure 2.1: Diameter changes of the CMPs during backfilling
After Mai et al. (2013)

Figure 2.2 shows the vertical and horizontal diameter changes of the CMPs covered by 0.6 m thick backfill, which are nonlinear. The deflections of the CMP with extensive corrosion were considerably larger than those of the CMP with light corrosion. Both CMPs had initially stiffer behavior until the applied force reached 40 kN. After 40 kN, the rate of diameter changes dramatically increased for both CMPs.

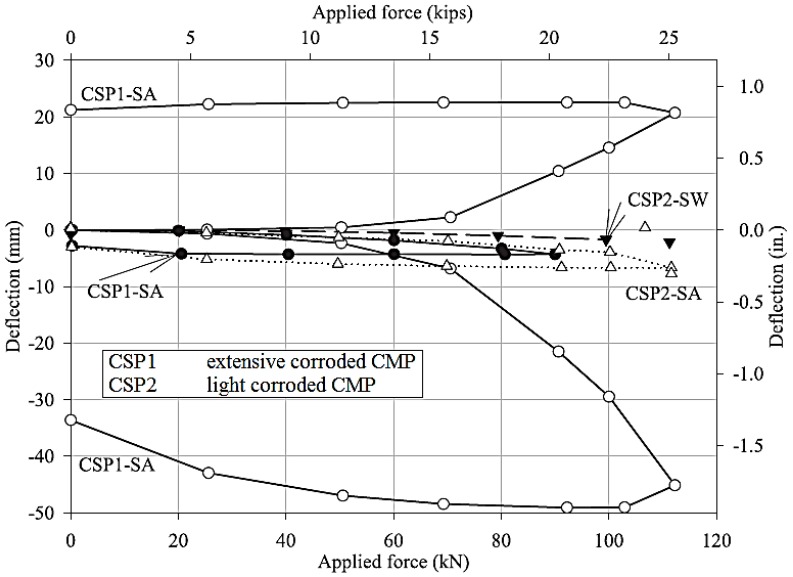

Figure 2.2: Diameter changes of the CMPs under surface loading
After Mai et al. (2013)

2.3 Smith et al. (2015)

Smith et al. (2015) investigated the effect of grout strength on the load-carrying capacity and stiffness of sliplined corrugated steel pipes using two-point loading tests. The corrugated steel pipes and HDPE liners had an internal diameter of 0.90 m and an external diameter of 0.78 m, respectively. A low-strength grout and a high-strength grout were used in this study. The average compressive strengths of the low-strength and the high-strength grouts were 1.3 and 31.7 MPa, respectively. In their study, the liners were placed at the center of the existing steel pipes. Figure 2.3 shows the applied load versus vertical and horizontal diameter changes for the intact steel pipe and the sliplined pipes with the low- or high-strength grout between the pipe and the liner. The vertical and horizontal diameter changes for each pipe were of approximately similar magnitude but with opposite signs. The test results showed that the sliplined steel pipe with the low-strength grout increased the pipe load-carrying capacity by more than three times as compared with the unlined pipe. Moreover, the use of the high-strength grout increased the pipe load-carrying capacity by more than 10 times as compared with the capacity of the unlined pipe. Figure 2.4 shows the applied load versus vertical and horizontal diameter changes for the rehabilitated steel pipes with and without liners. The results indicate that the liner had no effect on the load-carrying

capacity of the rehabilitated steel pipe with the high-strength grout. However, the liner increased the load-carrying capacity of the rehabilitated steel pipe with the low-strength grout by approximately 60%.

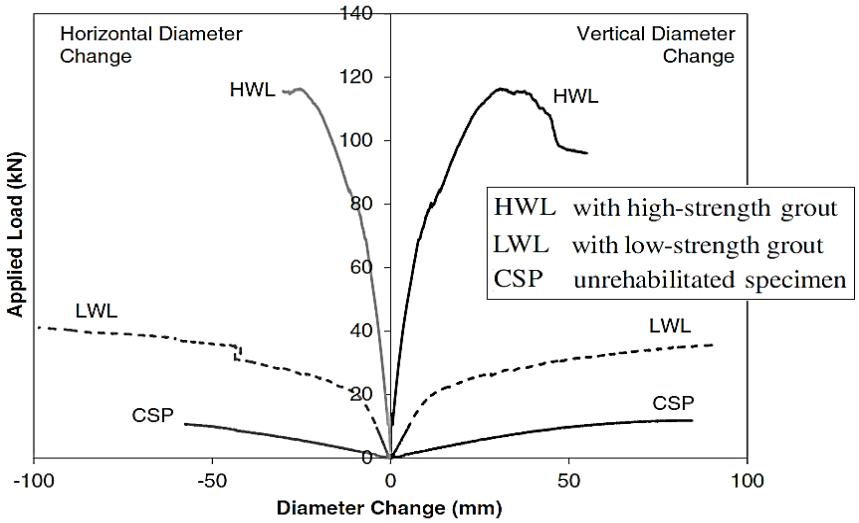

Figure 2.3: Applied load versus diameter changes for the intact and sliplined steel pipes
After Smith et al. (2015)

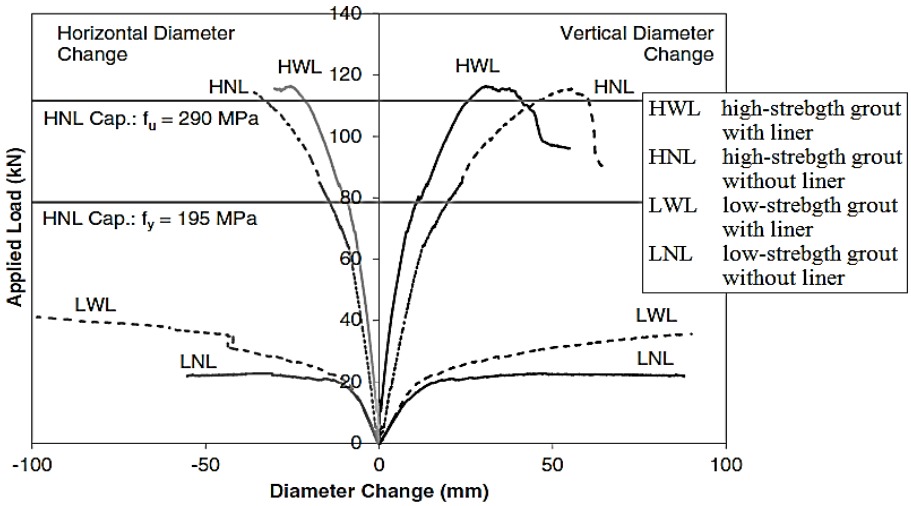

Figure 2.4: Applied load versus diameter changes of rehabilitated steel pipes with and without a liner
After Smith et al. (2015)

Smith et al. (2015) used a plasticity approach, whereby the load carrying capacity is calculated as the load required to form a plastic collapse mechanism. Smith et al. (2015) developed the following equation to calculate the maximum vertical load that can be applied onto the pipe:

$$P = \frac{M_{p,crown}}{R} + \frac{M_{p,invert}}{R} + \frac{2M_{p,spring\ line}}{R}$$ **Equation 2.1**

Where:

P = maximum applied load;

$M_{p\ crown}$, $M_{p\ invert}$, and $M_{p\ sringline}$ = plastic moment capacities of the pipe at the crown, invert, and springlines, respectively;

R = radius of the pipe taken to the centroid of the pipe wall.

For pipes with an identical cross section around their circumference, the following equations can be used:

$$P = \frac{4\ M_p}{R}$$ **Equation 2.2**

$$M_p = f_y Z$$ **Equation 2.3**

Where:

M_p = plastic moment capacity of the corrugated steel section;

f_y = yield strength of the material; and

Z = plastic modulus.

Since the moment capacities at the invert and crown for the sliplined pipes are different from the moment capacity at the springline, Equation 2.1 should be used. If the grout cracks, only the pipe remains to take the bending moment. Therefore, the plastic moment capacity (Mp) can be calculated using Equation 2.3. This approach also conservatively neglects the presence of the liner.

2.4 Simpson et al. (2015)

Simpson et al. (2015) investigated the performance of two sliplined buried corroded corrugated steel pipes under static surface loading. The steel pipe and the HDPE liner had a diameter of 1.80 and 1.52 m, respectively. The steel pipe had light corrosion on both sides of the invert. The average corrosion of the steel pipe was 13.5%. A neat grout with an average 28-day compressive strength of approximately 30 MPa was used. The fill material was a poorly-graded sandy gravel, which is classified as A-1 by AASHTO. Figure 2.5 shows the percent of the vertical diameter change under surface loading before and after sliplining. The results indicate that the sliplined steel pipe was more than 90% stiffer than the unlined pipe, so the diameter changes under surface loading decreased. Moreover, the sliplined steel pipe behaved as a semi-rigid pipe.

Simpson et al. (2015) found that the critical response areas for the corrugated steel pipes before and after sliplining occurred in the upper shoulder and crown region. In addition, the increased stiffness of the sliplined steel pipe resulted in less load being spread to the surrounding soil.

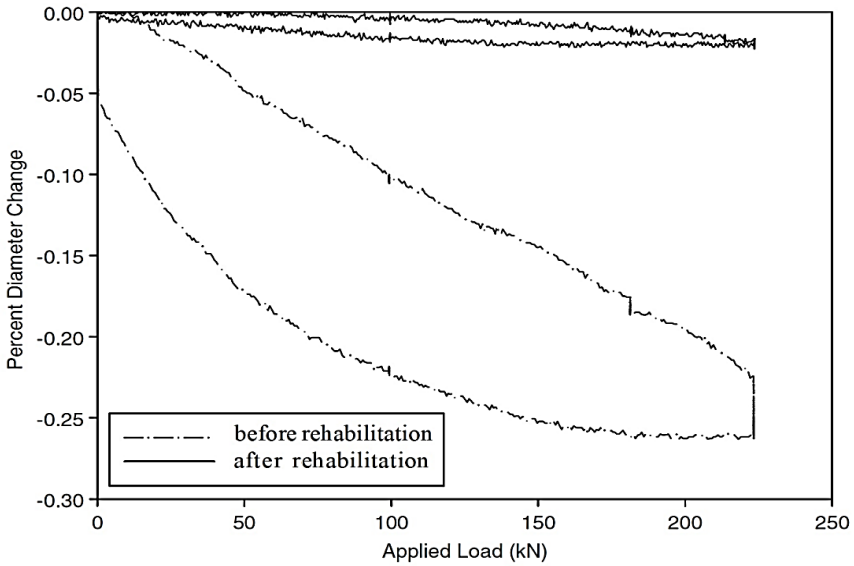

Figure 2.5: Vertical diameter change versus applied load before and after sliplining
After Simpson et al. (2015)

2.5 Tetreault (2016)

Tetreault (2016) investigated the effect of sliplining on the performance of two buried corrugated steel pipes under single wheel pair loading with a 0.45 m thick cover. The sliplined pipes were loaded to their ultimate capacities. The corrugated steel pipes had a diameter of 0.9 m, a length of 3 m, and an intact wall thickness of 1.6 mm. An HDPE pipe with an outer diameter of 772 mm and a wall thickness of 43 mm was used as a liner. Backfilling was undertaken using a poorly-graded sandy gravel classified as A-1 by AASHTO. Tetreault (2016) found that sliplining with a low-strength grout and a high-strength grout provided strengths well beyond the requirements. However, the sliplined pipe with the low-strength grout behaved rigid under a service load of 71 kN and flexible under a load of 350 kN.

2.6 Simpson et al. (2017)

Simpson et al. (2017) conducted an experimental study to evaluate the performance of two damaged reinforced concrete pipes in soil under surface loading before and after sliplining. They found that sliplining increased the stiffness of the pipes significantly and reduced the vertical diameter deformations by 87% to 93%.

Chapter 3: Behavior of Sliplined Corrugated Steel Pipes under Parallel-Plate Loading

3.1 Introduction

This chapter is to evaluate the effect of sliplining rehabilitation on the behavior of corroded corrugated steel pipes under parallel-plate loading in air, including load-carrying capacity and stiffness, vertical and horizontal diameter changes, and average strain and curvature of pipes. Seven parallel-plate loading tests were conducted on corrugated steel pipes with different degrees of corrosion using a universal testing machine.

3.2 Experimental Tests

3.2.1 Test Apparatus

Figure 3.1 shows the universal testing machine with a load capacity of 534 kN used to apply vertical loads on corrugated steel pipes. Khatri et al. (2013) used the same machine to evaluate the behavior of steel-reinforced high-density polyethylene pipes.

3.2.2 Steel Pipes and Liner

The corrugated steel pipe sections had a nominal inside diameter of 300 mm and a length of 455 mm, which satisfy the required dimensions for parallel-plate loading tests according to ASTM D2412-11 (ASTM, 2018). The pipe sections had a nominal wall thickness of 2 mm with a corrugation height of 15 mm and a corrugation length of 70 mm. The corrosions in steel pipes were simulated by cutting out some steel segments along the invert of the pipes. These segments represent the areas where water is trapped between two consecutive inner corrugation crests at invert and cannot drain through the pipes. The trapped water increases the rate of steel corrosion in these areas and results in complete corrosion. Figure 3.2 shows water remaining inside the corrugated pipe, which causes corrosion to the pipe.

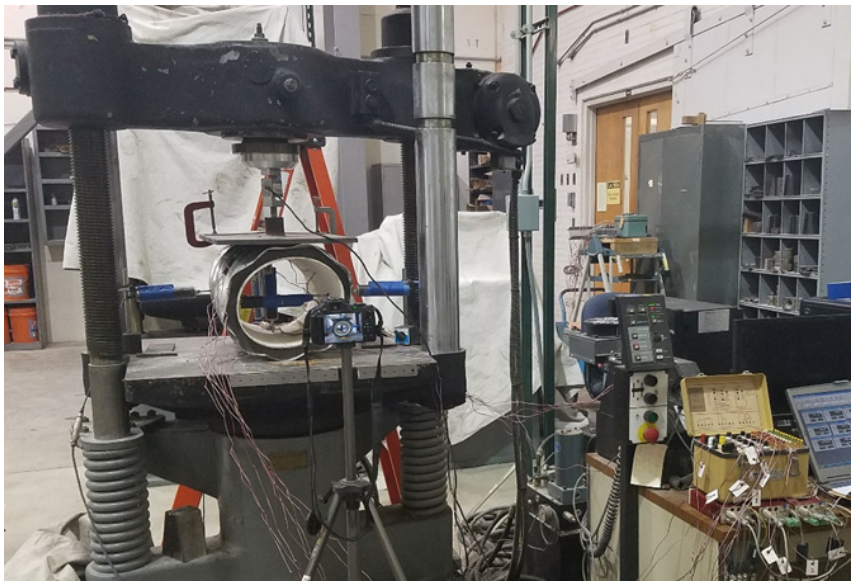

Figure 3.1: The universal testing machine and test setup for a parallel-plate loading test

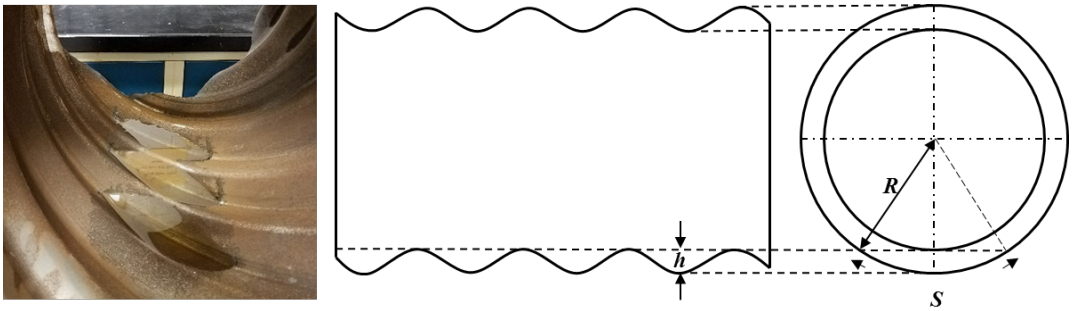

(a) (b)

Figure 3.2: Possible Corrosion Areas

(a) Water Remaining Inside the Corrugated Pipe; (b) Schematic Cross-Sections of the Corrugated Steel Pipe

The arc length of the corroded segment on a corrugated steel pipe can be estimated using the following equation:

$$S = 0.035\,R\ arcsin\sqrt{1-\frac{(R-h)^2}{R^2}} \qquad \textbf{Equation 3.1}$$

Where:

S = the arc length of the deteriorated segment of the pipe,

R = the outside radius of the pipe, and

h = the corrugation height.

The average cutout areas along the invert of two steel pipes in this study were 50% and 90%, which represent 50% and 90% degree of corrosion, respectively. Figure 3.3 shows these

pipes after the removal of the segments. PVC pipes with an inside diameter of 254 mm, a wall thickness of 3 mm, and a length of 455 mm were used as liners. These pipe liners were flexible. Figure 3.4 presents the applied load versus diameter change for the PVC liner, indicating a linear load-diameter change relationship. Moreover, at the same applied load, the vertical diameter change was larger than the horizontal one with a ratio of 1.33. The load-carrying capacity of the liner at 5% vertical diameter change (approximately 12.8 mm, typically used as a serviceability criterion in the practice for flexible pipes), was approximately 0.2 kN.

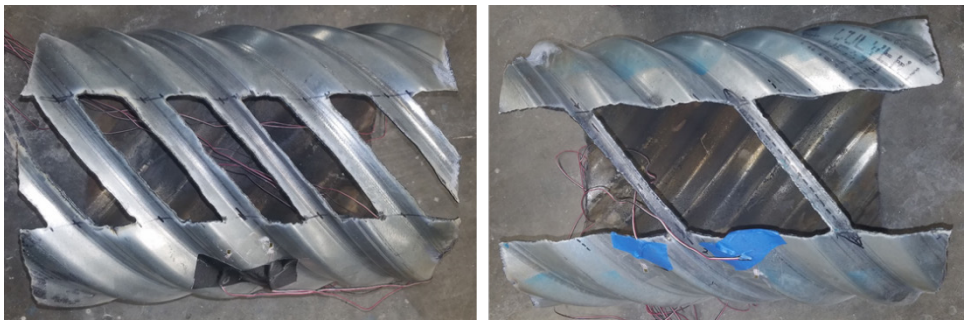

(a) (b)

Figure 3.3: Corrugated Steel Pipes with Simulated Corrosion: (a) 50% Cutout and (b) 90% Cutout

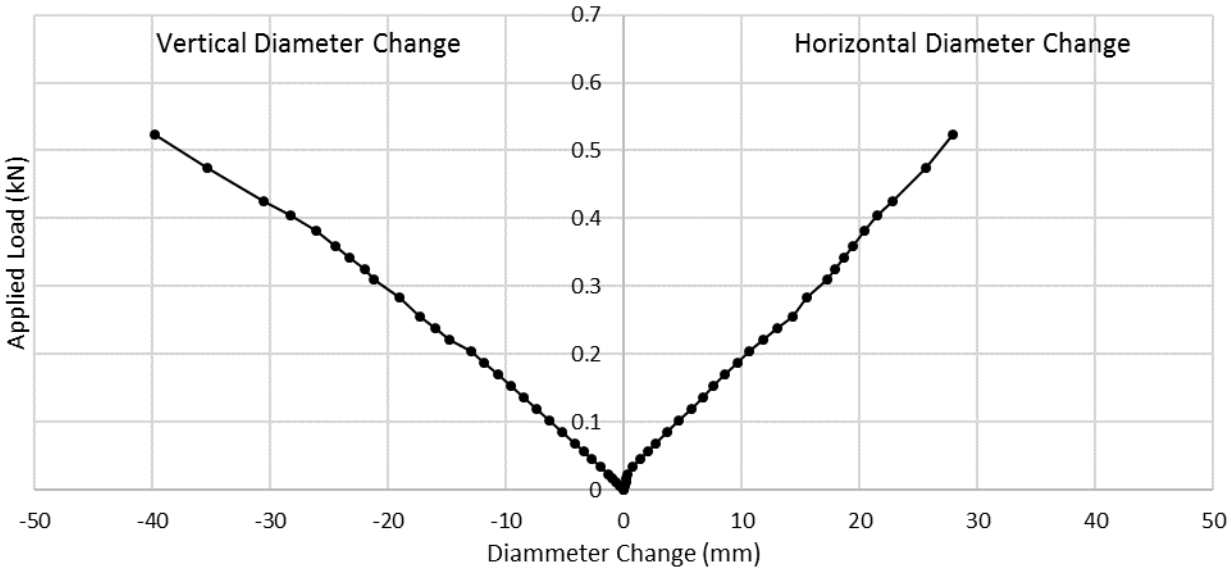

Figure 3.4: Applied load versus vertical and horizontal diameter changes of the liner

3.2.3 Grout

A low-strength, normal density grout was used in this study. This grout was prepared according to Ballinger and Drake (1995). The mix included 59 kg/m^3 cement, 178 kg/m^3 fly ash, 1542 kg/m^3 sand, and 265 liter water. Three unconfined compression tests were conducted on cylindrical concrete specimens with a diameter of 100 mm and a height of 200 mm using the ASTM C39/C39M standard (ASTM, 2004). The average seven-day compressive strength was 249 kPa and the density was 2126 kg/m^3. In this study, the sliplined pipes after grouting were kept in a curing room for seven days before the parallel-plate loading tests. Before grouting, the pipes were wrapped with a thin plastic sheet and a tape to keep the grout between the steel pipe and the liner.

3.2.4 Measurements

The applied load was measured using an S-shape load cell with a capacity of 40 kN. The vertical and horizontal diameter changes of the steel pipes and the liners were measured using two types of displacement transducers (DTs) with displacement limits of 100 mm and 50 mm, respectively. The intact and cut steel pipes were instrumented with 10 and eight foil electrical resistance strain gauges, respectively. The strain gauges were attached at both the crest and valley of the outside surface of a corrugation of the steel pipe so that the average strain and curvature of the pipe could be calculated as shown in Figure 3.5. The strain gauges had a gauge length of 5 mm and an electrical resistance of 120 Ω.

Figure 3.5: Strain gauges at both the crest and valley of a corrugation in the transversal direction of the pipe

3.2.5 Test Configurations

Figure 3.6 shows the schematic cross-section of the test setup, including the locations of the load cell, displacement transducers, and strain gauges. On the top of the pipe, a rigid plate was used to apply the load to the pipe. Three series of tests were conducted in this study. The first series of tests, Series A, were conducted on the simulated corroded steel pipes without a liner as shown in Figure 3.6(a). In these tests, the steel pipes had 0%, 50%, and 90% cutout, where the 0% cutout represents an intact steel pipe. In the second series of tests, Series B, three tests were carried out on sliplined steel pipes with 0%, 50%, and 90% cutout as shown in Figure 3.6(b). In these tests, the liners were placed on the invert of the steel pipes. In the third series, Series C, the liner was placed in the center of the steel pipe with 0% cutout, which was tested to evaluate the effect of the location of the liner or the area of grout as shown in Figure 3.6(c).

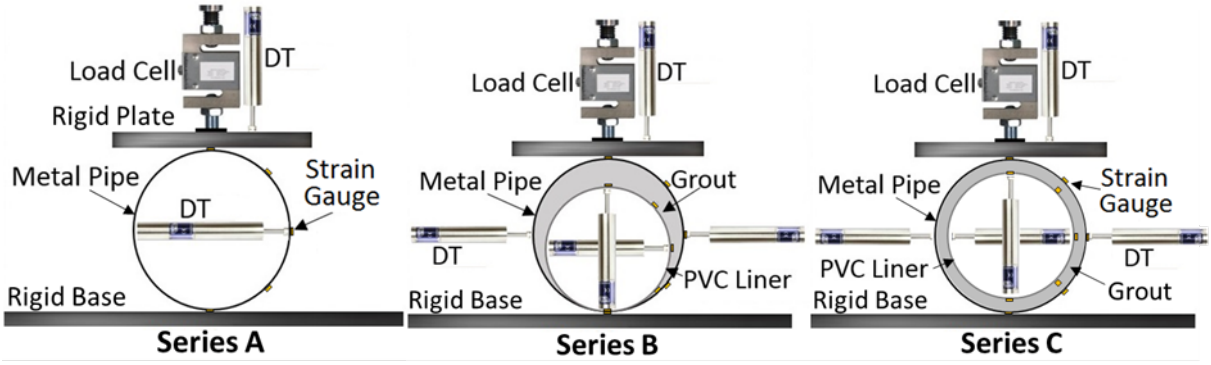

Figure 3.6: Test Configurations

(a) Series A – Steel Pipes Without a Liner; (b) Series B – Sliplined Steel Pipes With a Liner on the Invert; (c) Series C – Sliplined Steel Pipe With a Liner in the Center

3.3 Results and Discussion

3.3.1 Diameter Changes

Figure 3.7 shows the applied load versus diameter change curves for the steel pipes. During loading, the distance between the crown and the invert decreased in the direction of the applied load. However, the distance between the springlines increased. In the Series A tests, the vertical and horizontal diameter changes of the steel pipes without a liner were almost equal but in the

opposite direction (Figure 3.7). The unlined steel pipes with 0% cutout had higher load capacities than the pipes with 50% and 90% cutout. When the applied load was lower than 1.5 kN, the steel pipe with 50% cutout behaved stiffer than the pipe with 90% cutout. However, after 1.5 kN, the pipe with 90% cutout behaved stiffer than the pipe with 50% cutout. This phenomenon resulted from the fact that the pipe with 90% cutout behaved like an arch with a flat base as discussed below. The load-carrying capacities of the unlined corrugated steel pipes with 0%, 50%, and 90% cutout at 5% vertical diameter change (approximately 15 mm) were 9.0, 6.5, and 7.5 kN, respectively. In addition, the load-carrying capacity of the unlined corrugated steel pipe with 0% cutout was approximately 45 times higher than the PVC liner at the same vertical diameter change.

Machelski et al. (2009) developed the following equation to calculate the vertical deflections at the crown of corrugated steel arch culverts under vertical loading:

$$w = \alpha \frac{L^3}{EI} Q \qquad \textbf{Equation 3.2}$$

Where:

w = the vertical deflection at the crown;

α = the characteristic variable dependent on the geometry of the structure and the flat base support level;

L = the length of the culvert;

Q = the external load; and

EI = the bending stiffness of the corrugated steel plate.

Figure 3.8 shows the applied load versus diameter change for the steel pipe with 90% cutout and a corrugated steel arch culvert. Figure 3.8 shows the calculated result for the corrugated arch culvert with an open base having a central angle (ϕ) of 52°. This angle corresponds to the removed segments in the steel pipe with 90% cutout. At the beginning of loading up to approximately 1.5 kN, the vertical diameter change of the pipe increased quickly due to the flattening of the pipe at the bottom. After the bottom of the pipe became flat, the stiffness of the steel pipe with 90% cutout is similar to that of a corrugated steel arch culvert calculated using the Machelski et al. (2009) formula. This comparison indicates that the steel pipe with 90% cutout behaved as an arch.

Figure 3.9(a) shows the applied load versus the outside vertical and horizontal diameter changes that were measured by DTs installed outside the sliplined pipes in the test Series B and C.

In Series B, the sliplined steel pipe with 0% cutout had equal magnitude of outside vertical and horizontal diameter changes, but with opposite signs. However, the pipes with 50% and 90% cutout had larger outside vertical diameter changes than outside horizontal diameter changes at the same applied load. Figure 3.9(b) shows the applied load versus the inside vertical and horizontal diameter changes that were measured by DTs installed inside of the liner in the test Series B and C. In the sliplined pipes, the inside vertical diameter changes were larger than the inside horizontal diameter changes. For this series of tests, the load-carrying capacities of the sliplined steel pipes with 0%, 50%, and 90% cutout at 5% vertical diameter change were 16.0, 10.0, and 3.5 kN, respectively. In other words, the sliplined steel pipe with a lower degree of cutout had a higher load-carrying capacity than the pipe with a higher degree of cutout. The permanent outside vertical diameter changes for both the sliplined steel pipes with 0% and 50% cutout after unloading were approximately 23.5 mm.

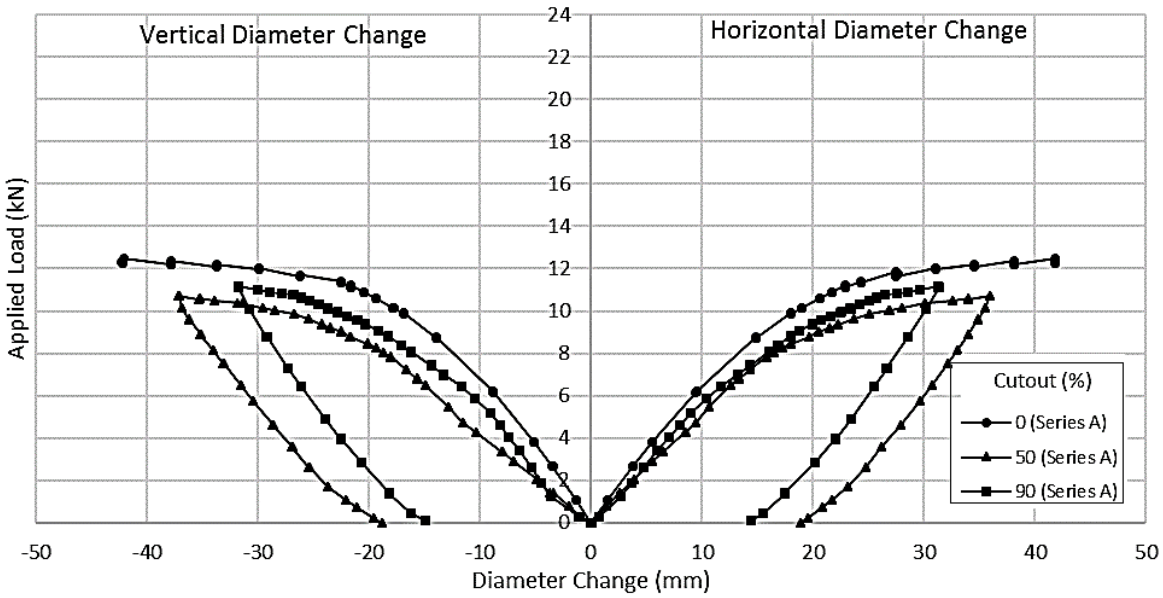

Figure 3.7: Applied load versus vertical and horizontal diameter changes in test Series A

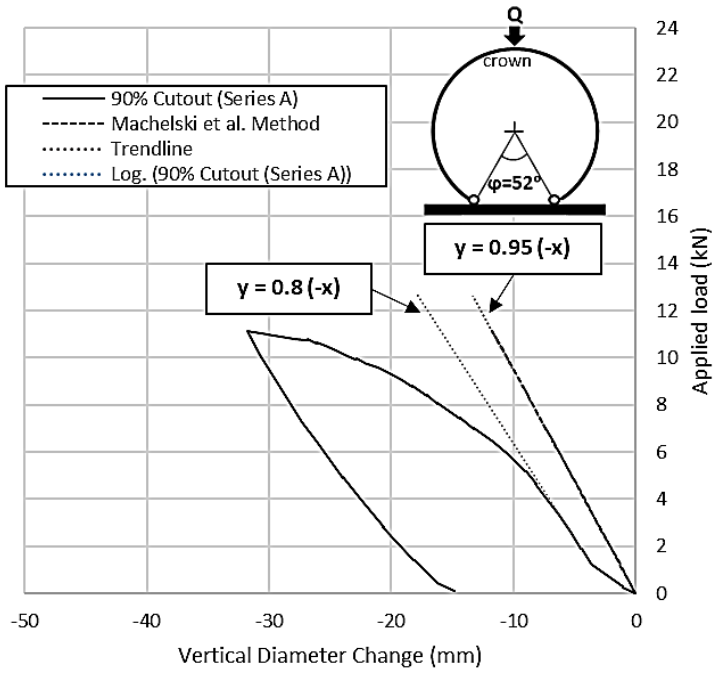

Figure 3.8: Applied load versus vertical diameter change on the unlined steel pipe with 90% cutout and the corrugated steel arch culvert

Figures 3.7 and 3.9(a) indicate that the sliplining rehabilitation increased the load-carrying capacities of the unlined steel pipes with 0% and 50% cutout. For instance, at 5% vertical diameter change, the load-carrying capacities of the steel pipes with 0% and 50% cutout were increased by 43.7% and 35.0%, respectively. Since the unlined steel pipes with 90% cutout performed as an arch structure, sliplining did not increase the load-carrying capacity of the steel pipes with 90% cutout.

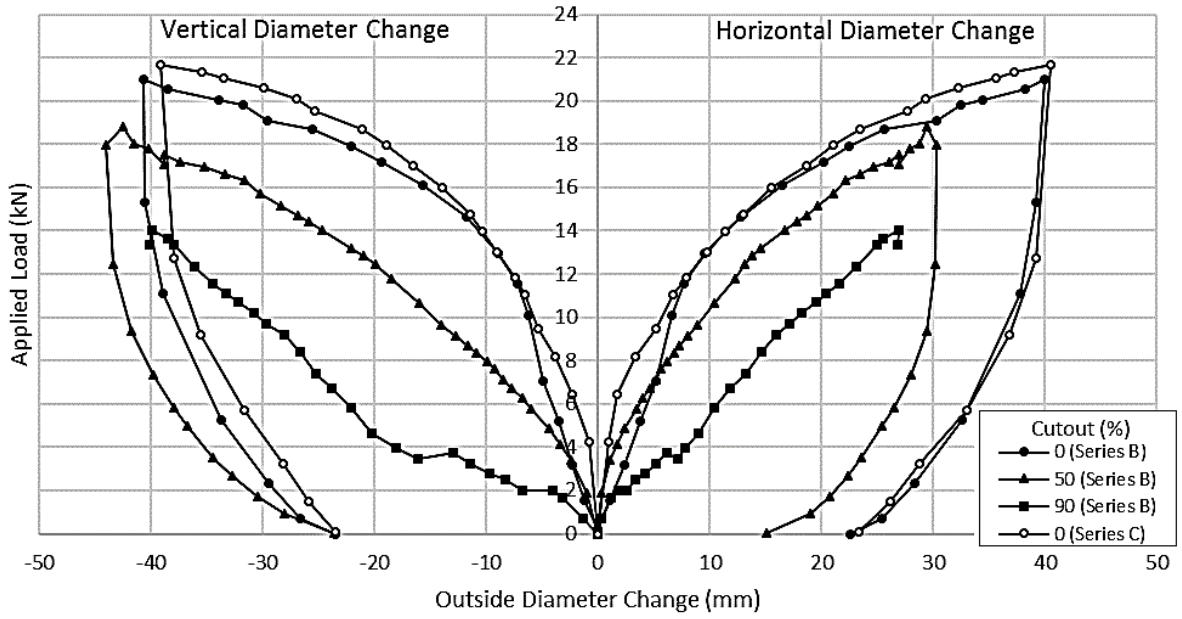

(a)

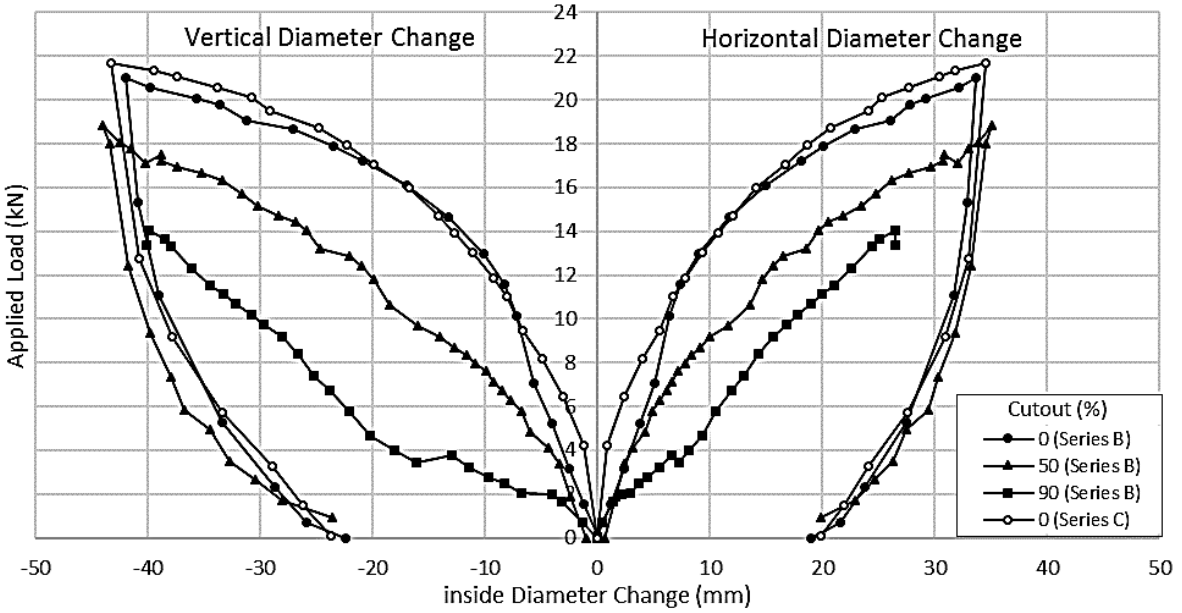

(b)

Figure 3.9: Applied load versus vertical and horizontal diameter changes: (a) outside diameter changes in test Series B and C, and (b) inside diameter changes in test Series B and C

The sliplined steel pipes with 0% cutout in the test Series B and C had similar load-carrying capacities, and vertical and horizontal diameter changes. For instance, at 5% vertical diameter change, the load-carrying capacity of the sliplined steel pipe with 0% cutout in the test Series C

was approximately 3.0% higher than that in the test Series B. However, placing a liner on the invert of the steel pipe may provide better drainage in practice than placing it in the center.

Table 3.1 shows the load-carrying capacities of the sliplined and unlined steel pipes, and PVC liner at 5% vertical diameter change in steel pipes (approximately 15 mm). The load-carrying capacity of the grout could be estimated as the differential capacity between the sliplined pipe and its components. For instance, the load-carrying capacity of the sliplined steel pipe with 50% cutout was 10.0 kN. The load-carrying capacities of the unlined steel pipe and the liner were 6.5 and 0.22 kN, respectively. Therefore, the load-carrying capacity contributed by grout was 3.28 kN (= 10.0 - 6.5 - 0.22). This result shows that the liner had the least contribution in the load-carrying capacity of the sliplined pipe. In the test where the liner was placed in the center of the steel pipe (series C), the grout carried a higher load than the grout in the test where the liner was placed on the invert (series B). In addition, the grout in the sliplined steel pipe with 0% cutout carried more load than the grout in the sliplined steel pipe with 50% cutout. However, because of the arch effect of the unlined steel pipe with 90% cutout, the load carried by the grout in the sliplined steel pipe with 90% cutout could not be calculated. The above results indicate that the degree of cutout and the location of the liner had an effect on the load-carrying capacity of the grout in the sliplined pipe.

Table 3.1: Load-carrying capacities of the sliplined pipe and its components at 5% vertical diameter change

Cutout (%)	Carried load (kN)			
	Sliplined steel pipe	Unlined steel pipe	PVC liner	Grout
0	16	9	0.22	6.78
	16.5*	9	0.22	7.28*
50	10	6.5	0.22	3.28
90	3.5	7.5	0.22	N/A

* Liner was placed at the center of the existing pipe.

3.3.2 Strains and Curvatures

The strains in the steel pipes were measured using strain gauges attached on the corrugation crest and the corrugation valley (Figure 3.5). The measured strains were used to calculate the average strain and curvature around the circumference of the steel pipes based on the equations

suggested by Simpson et al. (2015). The average strain in the steel pipe can be calculated using the following equation:

$$\varepsilon_{ave} = \varepsilon_1 - \frac{h+t}{2h}(\varepsilon_1 - \varepsilon_2) \quad \textbf{Equation 3.3}$$

Where:

ε_{ave} = the average strain;

ε_1 = the strain on the corrugation valley;

ε_2 = the strain on the corrugation crest;

h = the radial distance between strain gauges; and

t = the wall thickness.

The measured strains were also used to calculate the curvature of the steel pipe as follows:

$$\kappa = \frac{\varepsilon_2 - \varepsilon_1}{h} \quad \textbf{Equation 3.4}$$

Where:

κ = the curvature of the pipe.

Basically, the positive curvature represents a tensile strain on the outside surface and a compressive strain on the inside surface of the pipe. In this study, it was assumed that the distributions of the strain and curvature across the vertical centerline along the pipe cross-section were symmetric. Simpson et al. (2015) pointed out that the average strains and curvature profiles are not completely symmetric about the centerline even though the loading plate was placed along the centerline.

Figure 3.10 shows the calculated average strains and curvatures around the circumference of the unlined steel pipes in test Series A, under different applied loads. During loading, the negative strains were observed at the crown and invert of the steel pipes. However, the positive strains were localized at the springlines of these pipes. For instance, under the applied load of 11 kN, the maximum average positive strains in the pipes with 0%, 50%, and 90% cutout were approximately 0.2%, 0.42%, and 0.23%, respectively. At the same applied load, however, the maximum average negative strains at the crown of these pipes were -0.08%, -0.32%, and -0.14%, respectively. Moreover, Figure 3.10 indicates that the steel pipes with 0% and 50% cutout had significant bending moments developing around the springline region and the crown, respectively.

However, no significant bending moment was observed in the pipe with 90% cutout because of the arch effect of the unlined pipe with 90 % cutout.

Figure 3.11 shows the calculated average strains and curvatures around the circumference of the sliplined steel pipes in test Series B and C, under different applied loads. Similar to the unlined steel pipes during loading, the negative strains were observed at the crown and invert of the steel pipes. However, the positive strains were localized at the springlines of these pipes. For example, under the applied load of 11 kN, the maximum average positive strains in the steel pipes with 0%, 50%, and 90% cutout were approximately 0.11%, 0.13%, and 0.17%, respectively. These results show that after sliplining, the maximum average positive strains in the steel pipes with 0%, 50%, and 90% cutout were reduced by 45%, 69%, and 26%, respectively. At the same applied load, the maximum average negative strains at the crown of these pipes were -0.04%, -0.05%, and -0.13%, respectively. Moreover, after sliplining, the maximum average negative strains in the steel pipes with 0%, 50%, and 90% cutout were reduced by 50%, 84%, and 7%, respectively.

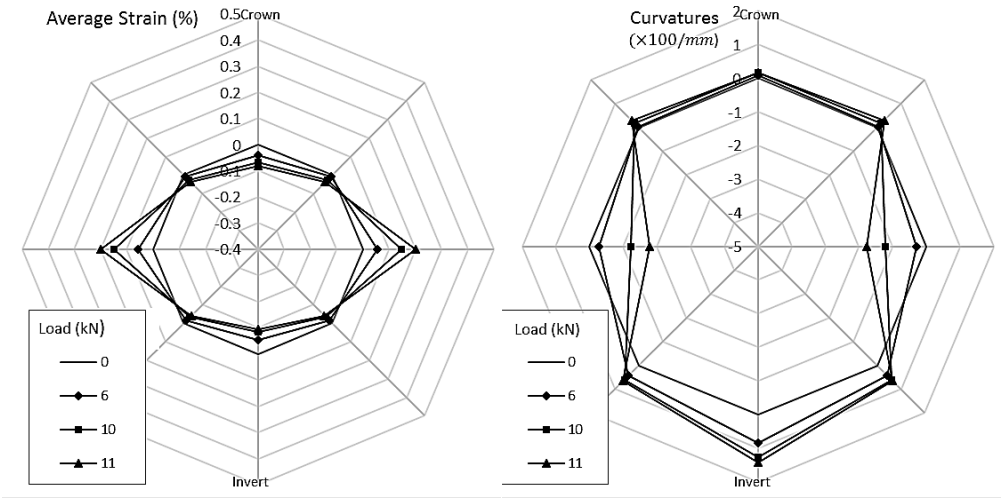

(a)

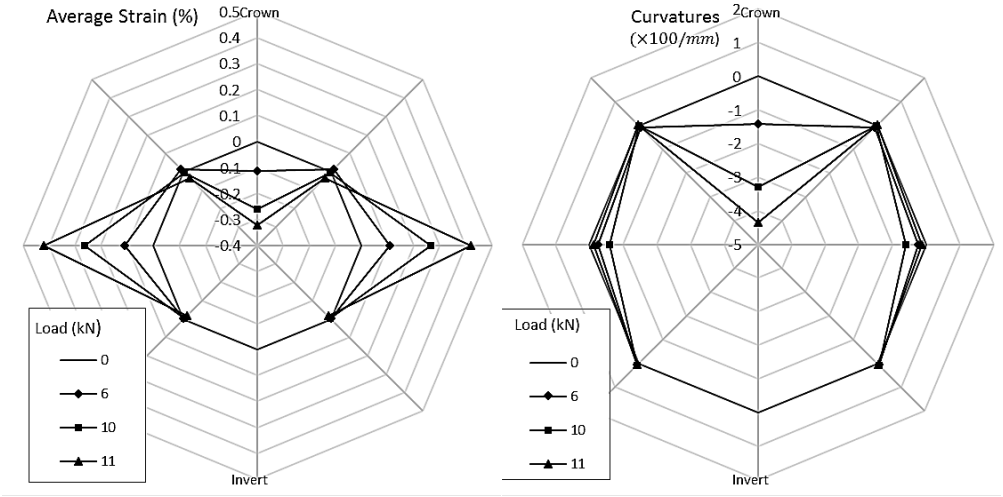

(b)

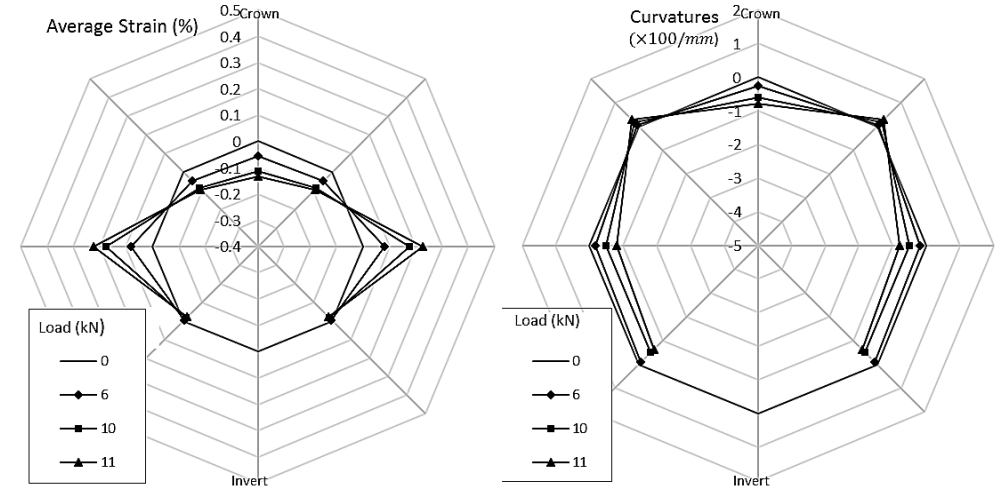

(c)

Figure 3.10: Average strains and curvatures around the unlined corrugated steel pipes in test Series A: (a) 0% cutout, (b) 50% cutout, and (c) 90% cutout

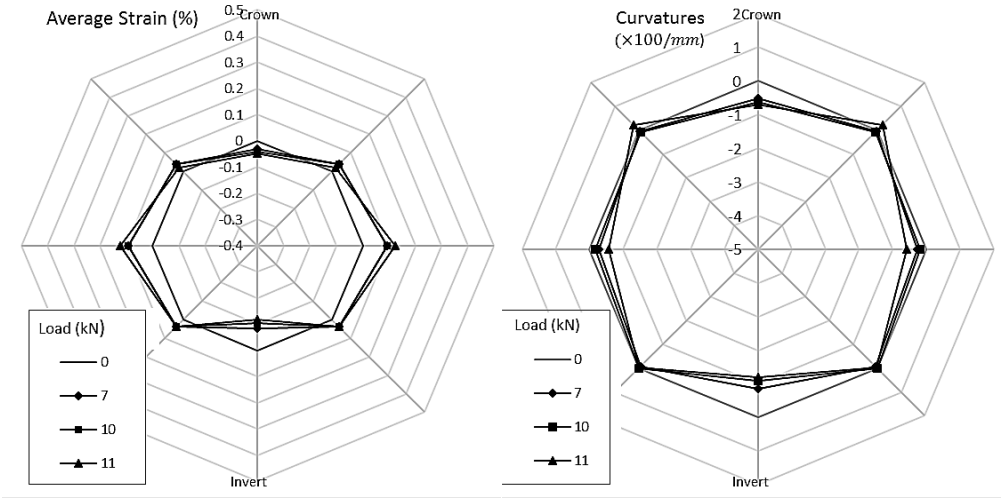

(a)

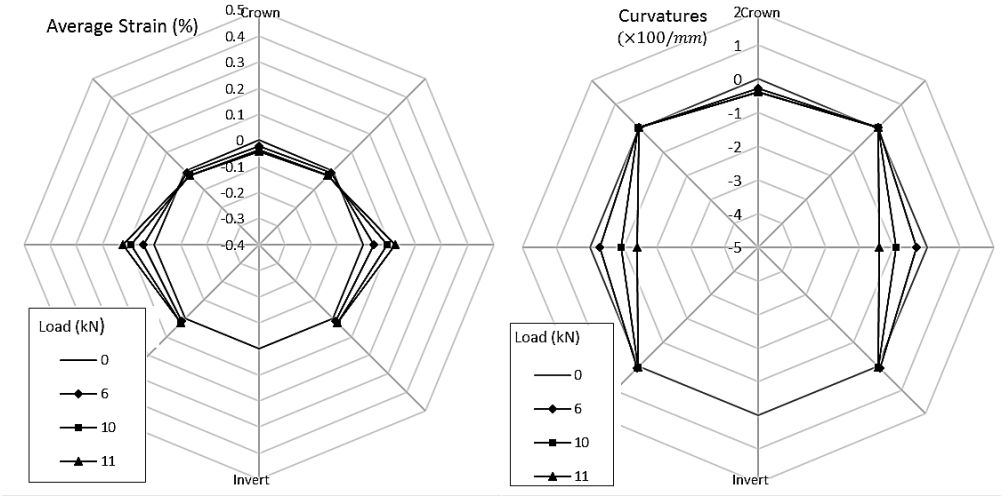

(b)

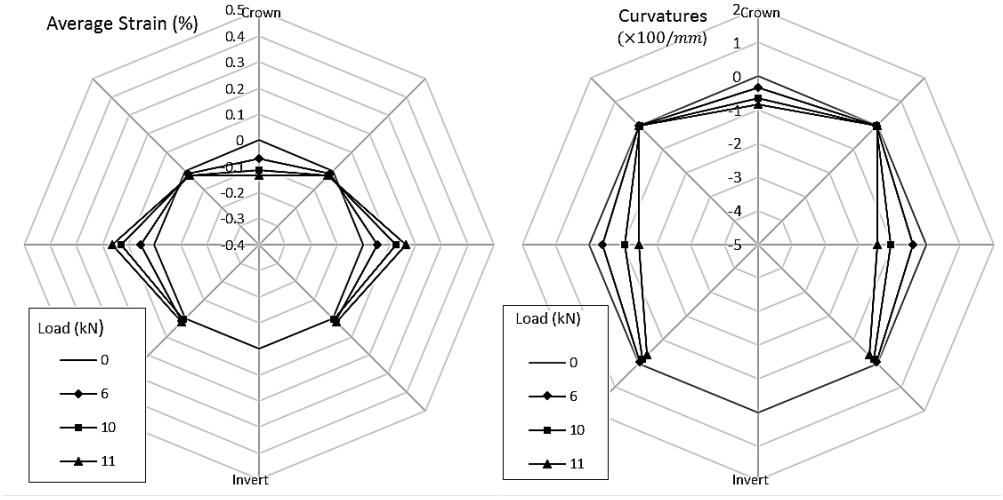

(c)

Figure 3.11: Average strains and curvatures around the sliplined steel pipes with: (a) 0% cutout in Series B, (b) 50% cutout in Series B, (c) 90% cutout in Series B, and (d) 0% cutout in Series C (Continued on next page)

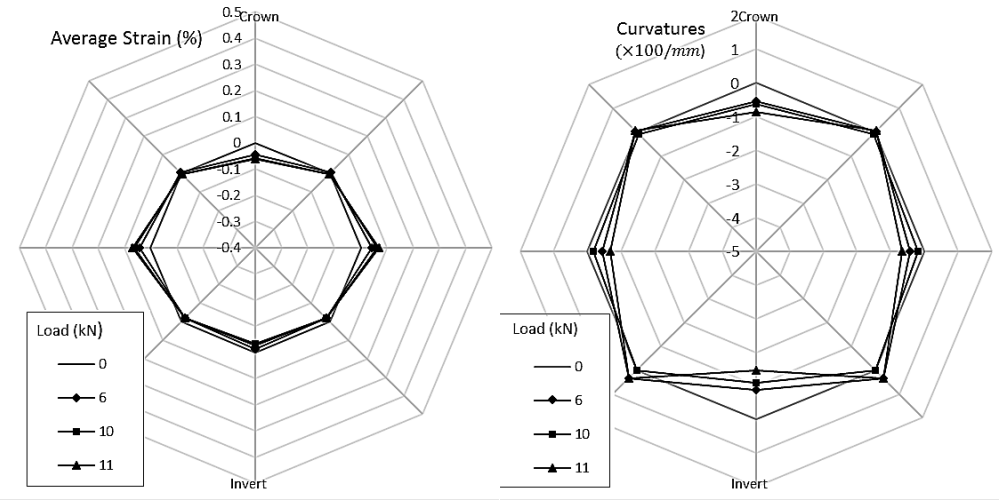

(d)

Figure 3.11: Average strains and curvatures around the sliplined steel pipes with: (a) 0% cutout in Series B, (b) 50% cutout in Series B, (c) 90% cutout in Series B, and (d) 0% cutout in Series C (continued)

Figures 3.11(a) and (d) show the differences between the average strains in the sliplined steel pipes with 0% cutout in test Series B and C. When the liner was placed on the invert (Series B), the maximum average positive strains at the springlines of the steel pipe were higher than those when the liner was placed in the center (Series C). For example, under the applied load of 11 kN, the maximum positive strains in the steel pipe in the test Series B and C were approximately 0.11% and 0.07%, respectively. The maximum average negative strain at the crown of the steel pipe in the test Series B was higher than that in Series C. However, the strain at the invert of the steel pipe in the test Series B was lower than that in Series C. For instance, under the applied load of 11 kN, the maximum average negative strains at the crown of the steel pipe in the test Series B and C were approximately -0.04% and -0.06 %, while those at the invert were -0.11% and -0.02%, respectively. Moreover, Figures 3.11(a) and (d) indicate that the sliplined steel pipes with 0% cutout (Series B and C) had significant bending moments developing in their invert region. However, the pipes with 50% and 90% cutout had bending moments developing in their springline region as shown in Figures 3.11(b) and (c).

Chapter 4. Field Evaluation of Sliplining Rehabilitation on Performance of Corroded Corrugated Steel Pipe

4.1 Introduction

This chapter contains an evaluation of the effect of sliplining on the behavior of a highly corroded corrugated steel pipe that was placed at a shallow depth under an asphalt pavement in the field. A series of truck loading and plate loading tests were conducted before and after the steel pipe being rehabilitated with a grouted HDPE liner to investigate: (1) load-carrying behavior and stiffness; (2) vertical and horizontal diameter changes; (3) average strain and curvature of pipes; and (4) settlement of the pavement surface. Furthermore, deformations, strains, and curvatures around the circumference of the liner were monitored during sliplining, service, and loading.

4.2 Description of Field Test

A corroded corrugated steel pipe located at a T intersection on the North 482 Road and the East 1250 Road (Old 59 Highway), Douglas County, KS, was selected to conduct the field study. The corroded corrugated steel pipe was located approximately 0.4 m beneath an asphalt pavement. The thickness and the width of the asphalt pavement was approximately 60 mm and 7.3 m, respectively. Figure 4.1(a) shows the steel pipe with high corrosion located at the haunch locations on either side of the invert and a completely lost invert. The Public Works Department of Douglas County, KS, sliplined the corroded corrugated steel pipe by driving two HDPE pipes directly through the existing steel pipe. One of the HDPE pipes was fully instrumented. The HDPE pipes were jointed mechanically using threaded male and female connectors. Then, the assembled liner was inserted inside the steel pipe using an excavator and positioned as shown in Figure 4.1(b), where the instrumentation was orientated. The erosion under the invert shown in Figure 4.1(a) was not treated before sliplining. Two pairs of wooden blocks above the liner were used to brace the liner inside the steel pipe to prevent uplift resulting from buoyancy during grouting. The wooden blocks were placed at both ends of the steel pipe. An insulating foam sealant was used to seal the annulus space between the steel pipe and the liner at both ends of the pipe to prevent grout from flowing out. At the north (the upstream) end of the steel pipe, a small segment of the crown was cut out to provide an access to grouting. Then, the space between the liner and the existing steel

pipe was grouted using a gravity grouting process in one lift as shown in Figure 4.1(c). Figure 4.2 illustrates schematic views of the cross-sections of the North 482 Road. The corroded corrugated steel pipe was subjected to plate and truck loading tests before and after sliplining. Figure 4.3 shows the air temperature variations during the construction and testing days.

(a) (b) (c)

Figure 4.1: Sliplining procedure: (a) corroded corrugated steel pipe; (b) installing a liner; and (c) grouting

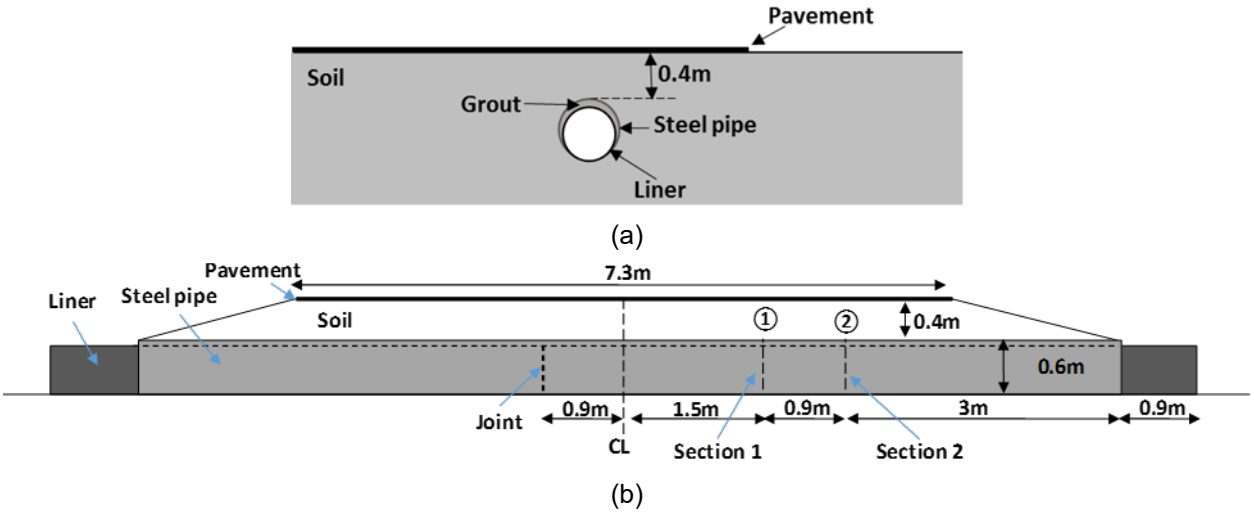

Figure 4.2: Schematic view of the cross-sections of the North 482 Road: (a) across the length and (b) across the width

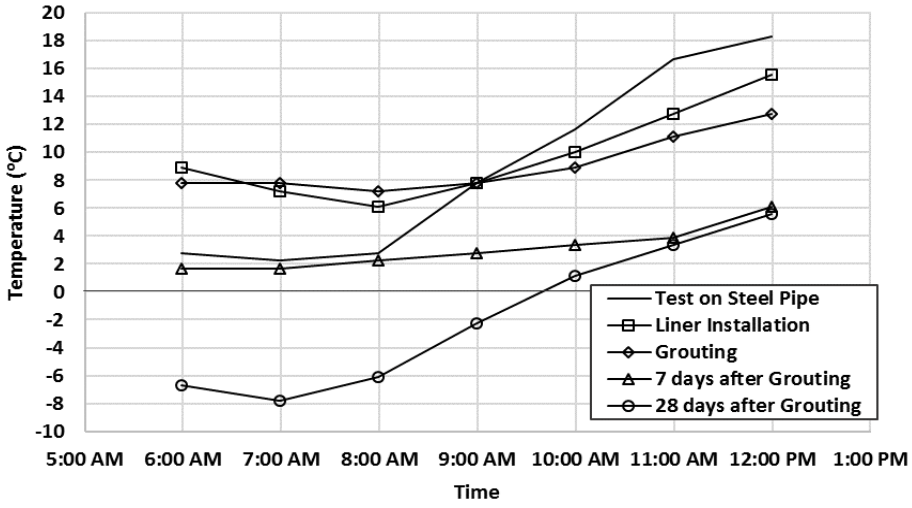

Figure 4.3: Air temperature variations during the construction and testing days

4.2.1 Soil

Dynamic Cone Penetration (DCP) testing was used to estimate the thicknesses and in-situ strengths of the base, subbase, and subgrade according to the ASTM D6951/D6951M (2015) standard. The DCP test measures the penetration rate of the DCP rod with an 8-kg hammer through undisturbed soil or compacted fill, or both. The DCP test was conducted at two locations: (1) directly above the location of the steel pipe and (2) approximately 2 m away from the pipe to the east side on an unpaved section of N 482 Road. To conduct the DCP test on the base material above the steel pipe, the asphalt pavement was removed to provide access to the base material. The DCP Penetration Index (DPI) was used to estimate the California Bearing Ratio (CBR) based on the equations suggested by ASTM D6951/D6951M (2015). Figure 4.4 presents the number of blows (N) versus the investigated depth (Z) under the asphalt pavement. The results of the DCP test in Figure 4.4(a) show two significant changes in the DPI values at depths of 60 and 220 mm. The changes indicate that the approximated thickness of the base, subbase, and subgrade were 60, 160, and 185 mm. The average CBR values of the base, subbase and subgrade were >100%, 65.8%, and 9.1%, respectively. The results of the DCP test in Figure 4.4(b) show that the unpaved section of the N 482 Road consisted of base and subgrade. The approximate thickness of the base was 85 mm. At the unpaved section, the average CBR values of the base and subgrade were >100% and 9.3%, respectively.

4.2.2 Steel Pipe

The existing corrugated steel pipe had a nominal inside diameter of 610 mm and a length of 11 m. It had a nominal wall thickness of 2 mm with a corrugation height of 15 mm and a corrugation length of 75 mm. The corrosion removed the entire wall of the pipe along the invert and reduced the wall thickness of the haunches. The average removed arc length of the wall of the pipe along the invert was approximately 210 mm as shown in Figure 4.1(a). The calculated arc length of the corroded segment on the corrugated steel pipe was 193 mm based on the following equation suggested by Rahmaninezhad et al. (2019):

$$S = 0.035\, R\ arcsin\sqrt{1 - \frac{(R-h)^2}{R^2}} \qquad \textbf{Equation 4.1}$$

Where:

S = the arc length of the corroded segment of the pipe,

R = the outside radius of the pipe, and

h = the corrugation height.

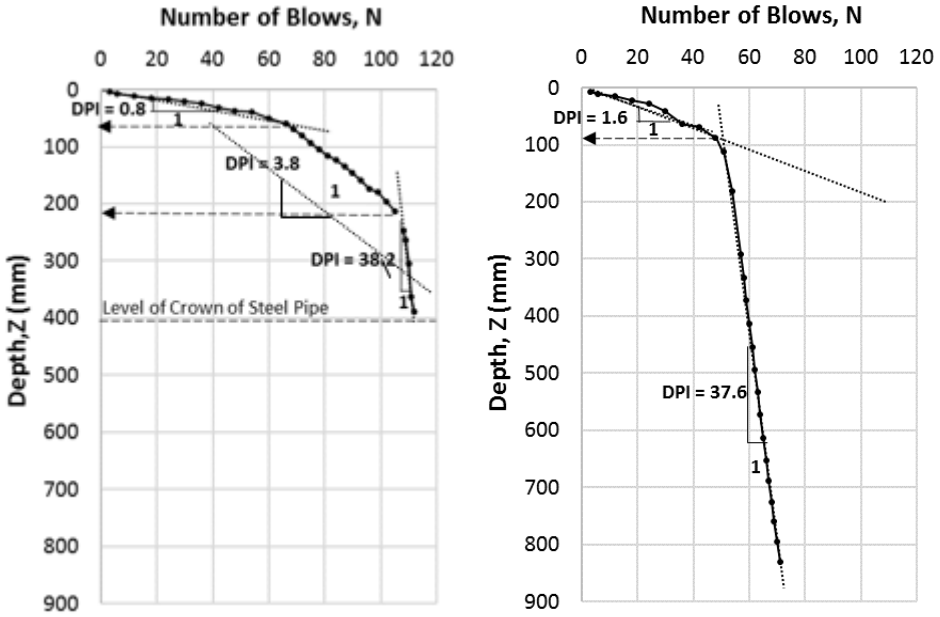

Figure 4.1. DCP test results: (a) above the pipe and (b) 2 m at the east-side of the pipe

4.2.3 HDPE Liner

Two HDPE pipes (22" OD DR32.5 M/F) manufactured by Snap-Tite were used as the liner. The HDPE pipes had average outer and inner diameters of 560 mm, and 541.6 mm, respectively, a wall thickness of 17.2 mm, and a length of 18.38 m.

4.2.4 Grout

A low-viscosity grout was used for sliplining. The mix included 254 kg/m^3 cement, 384 kg/m^3 fly ash, and 492 kg/m^3 water. Six cylindrical concrete specimens of 100 mm in diameter and 200 mm high were prepared in the laboratory. After the specimens were removed from the molds, height reductions of the specimens were observed. The average height reduction was approximately 19% of the original height. Unconfined compression tests were conducted on the concrete specimens using the ASTM C39/C39M (2004) standard. The average 7-day and 28-day compressive strengths were 2.7 MPa and 5.1 MPa, respectively.

4.2.5 Measurements

The applied loads for loading tests were measured using an S-shape load cell with a capacity of 50 kN. The vertical and horizontal diameter changes of the steel pipe and the liner, and the plate settlement were measured using two types of displacement transducers (DTs) with displacement limits of 100 mm and 50 mm. Figure 4.5 shows the positions of strain gauges, DTs, and location of the laser tape around the liner. The laser tape with an accuracy of 0.1 mm was used to measure the inner diameter changes of the liner. The laser tape was located on different positions inside the liner to measure the diameter changes in the horizontal direction, vertical direction, at angles of +45°, and -45° from the vertical as illustrated in Figure 4.5(a). The diameter at the angle of +45° represents the distance between the left shoulder and the right haunch while the diameter at the angle of -45° represents the distance between the right shoulder and the left haunch. The inner and outer faces of the liner at two sections were instrumented with 32 foil electrical resistance strain gauges as shown in Figure 4.5. The strain gauges had an electrical resistance of 120 Ω, a matrix length of 8.1 mm, a matrix width of 4.3 mm, and could measure strains up to ±3%.

4.3. Results and Discussion

4.3.1 Parallel-Plate Loading Test on Liner

The parallel-plate loading test was conducted to determine the load-deflection characteristics of the HDPE liner in accordance with the ASTM D2412-11 (2018). Figure 4.6(a) shows the schematic cross-section of the parallel-plate loading test setup, including the locations of the load cell and DTs. The test specimen was a piece of the HDPE pipe of 150 ± 3 mm long. Figure 4.7 presents the applied load versus diameter change for the HDPE liner, indicating the vertical diameter changes were larger than the horizontal diameter changes. The load-carrying capacity of the liner at 5% vertical diameter change (approximately 26.1 mm, typically used in practice for design of flexible pipes) was approximately 0.64 kN.

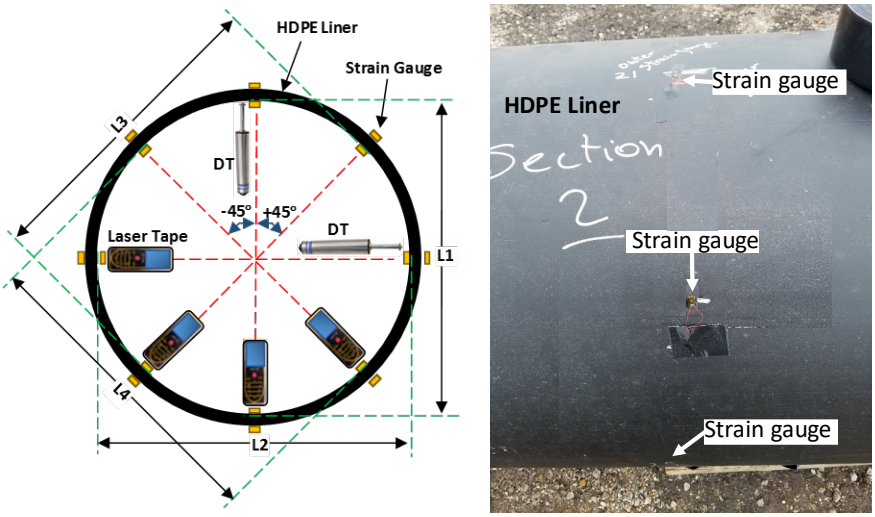

(a) (b)

Figure 4.5: Instrumentation: (a) positions of strain gauges, DTs, and laser tape (not to scale) and (b) an attached strain gauge on outer face of the liner

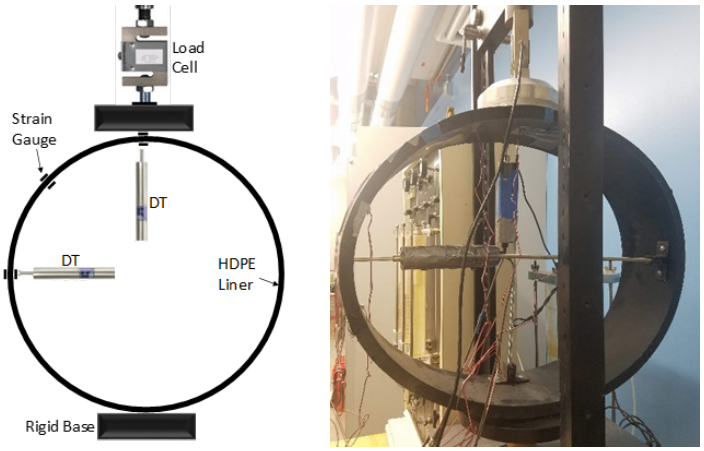

(a) (b)

Figure 4.6: Parallel-plate loading test: (a) schematic cross-section and (b) test setup

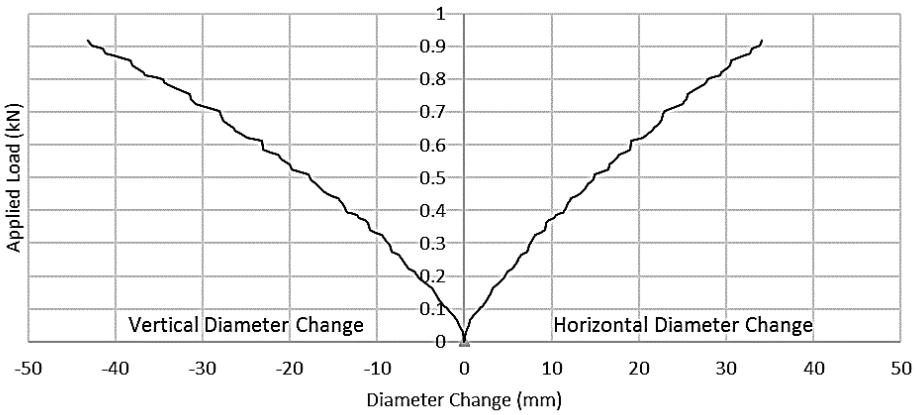

Figure 4.7: Applied load versus vertical and horizontal diameter changes of the liner

4.3.2 Liner Deformation and Strain

This section contains a presentation and discussion of the HDPE pipe deformations and strains before and after sliplining the corroded steel pipe. The measurements using the laser tape were utilized to evaluate the deformations of the liner at 7 days and 28 days after grouting. Figure 4.8 shows the radius changes of the liner at the locations of Section 1 and Section 2. The deformation profiles are not completely symmetric about the liner centerline. Rahmaninezhad et al. (2019) showed the helically-wound form of the corrugation with a sharp helix angle caused the asymmetric deformation in sliplined corrugated steel pipes. The results for both sections at 7 days after grouting show that the distance between the crown and the invert (L1) decreased, while the

distance between the springlines (L2) increased. Moreover, the diameters of the liner at +45° (L3) and -45° (L4) from the vertical decreased. In Section 1, the changes at L1, L2, L3, and L4 were -1.2, 2.1, -1.3, and -3.1 mm, respectively. In Section 2, the changes at L1, L2, L3, and L4 were -2.6, 3.7, -1.4, and -4.3 mm, respectively. The average diameter changes in Section 1 and Section 2 were -0.9 and -1.1 mm, respectively. However, at 28 days after grouting, the liner contracted. Since the average temperature during the measurement was -2 ℃ as shown in Figure 4.3, the radius changes of the liner might be influenced by freezing. The radius reduction of the liner might result from the water expansion within the grout after freezing. The average diameter changes in Section 1 and Section 2 were -8.2 and -7.6 mm, respectively, at 28 days after grouting.

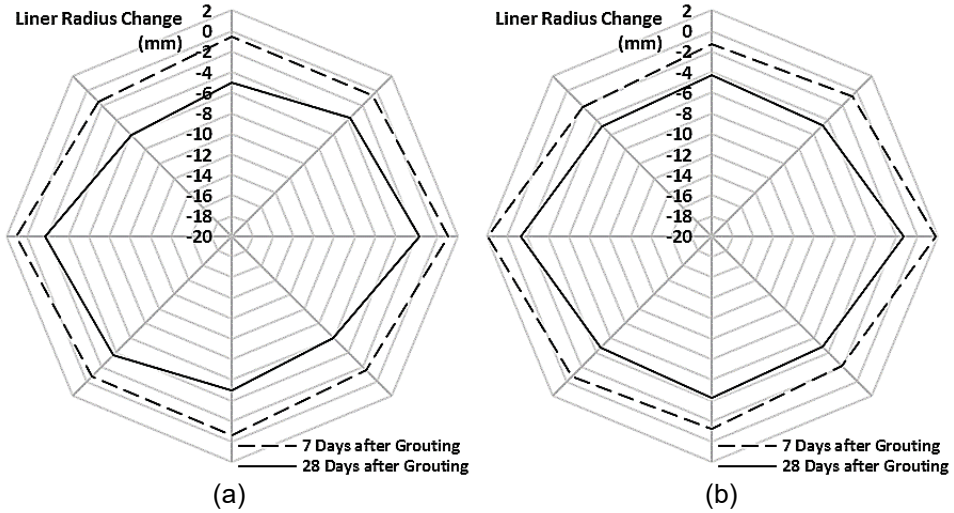

Figure 4.8: Radius changes for the liner: (a) Section 1 and (b) Section 2

The strains in the liner were measured using strain gauges attached on the inner and outer faces of the liner as shown in Figure 4.5. Unfortunately, some of the strain gauges attached on the outer face of the liner were broken during driving of the liner into the steel pipe. The measured strains were used to calculate the average strains and the curvatures around the circumference of the liner based on the equations suggested by Simpson et al. (2015). The average strain in the liner can be calculated using the following equation:

$$\varepsilon_{ave} = \frac{\varepsilon_1+\varepsilon_2}{2}$$ **Equation 4.2**

Where:

ε_{ave} = the average strain;

ε_1 = the measured strain of the inner face; and

ε_2 = the measured strain of the outer face.

Figure 4.9 shows the measured strains and calculated average strains around the circumference of the liner. Basically, the positive strain represents a tensile strain on the surface of the liner. Figure 4.9 indicates that the strain profiles are not symmetric about the liner centerline. This result may be attributed to a number of factors, such as the degree of corrosion and/or the deflection of the steel pipe, the variation in the grout thickness around the liner, and the heterogeneous nature of the surrounding soil. For example, in all stages of measurement, there was a localized average negative strain concentration at the right shoulder of the liner. After the liner was installed, a localized positive strain concentration occurred at the right haunch as shown in Figure 4.9(a). However, after grouting, the localized positive strain concentration was observed at the invert of the liner as shown in Figure 4.9(b). Grouting increased the average strain at the invert of the liner by approximately 102%. However, at the crown of the liner, the inner strain was reduced by approximately 87%. At 7 days after grouting, the average strains decreased and the liner was fully under compression as shown in Figure 4.9(c). Moreover, Figure 4.9(d) shows the liner underwent further compression at 28 days after grouting, which was partially related to water freezing within the surrounding grout.

The measured strains were also used to calculate the curvature of the liner as follows:

$$\kappa = \frac{\varepsilon_2-\varepsilon_1}{h}$$ **Equation 4.3**

Where:

κ = the curvature of the liner and

h = the liner wall thickness.

The positive curvature represents a tensile strain on the outside surface and a compressive strain on the inside surface of the liner. In all stages of the measurement, a notable negative bending moment was observed on the right shoulder of the liner. This bending moment might be a result of deformation at the same location on the steel pipe. Figure 4.10(a) shows that driving of the liner through the steel pipe generated positive curvatures at the invert, the right spring line, and the right

shoulder of the liner. However, no significant curvature occurred at the left springline and the left haunch. During the grouting process, the pressure induced by the grout generated a negative curvature at the invert of the liner as shown in Figure 4.10(b). At 7 days after grouting, the grout hardening caused a positive bending at the left springline and the left haunch as shown in Figure 4.10(c). Except for positive bending at the right shoulder induced during liner installation, no meaningful curvature was perceived at 28 days after grouting as shown in Figure 4.10(d).

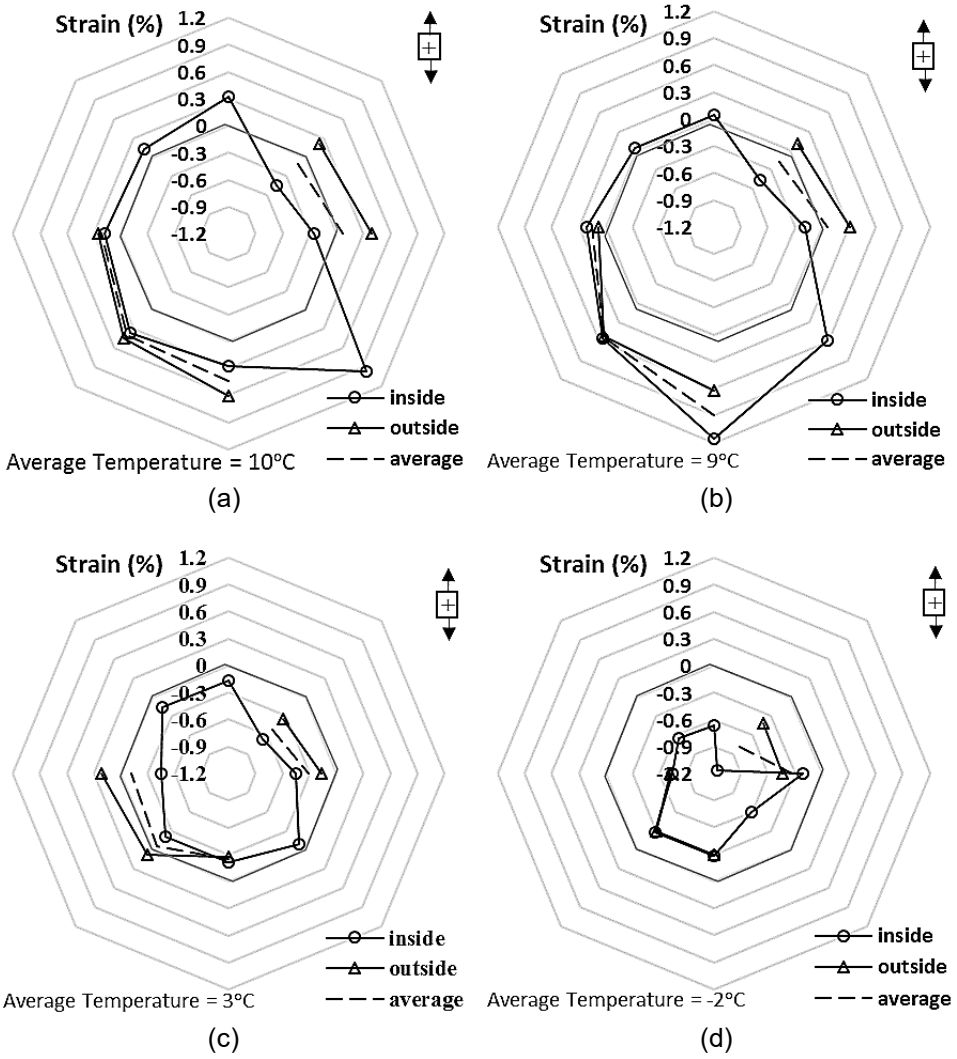

Figure 4.9: Inside, outside, and average strains around the liner at the locations of Section 1: (a) after liner installation; (b) after grouting; (c) at 7 days after grouting; and (d) at 28 days after grouting

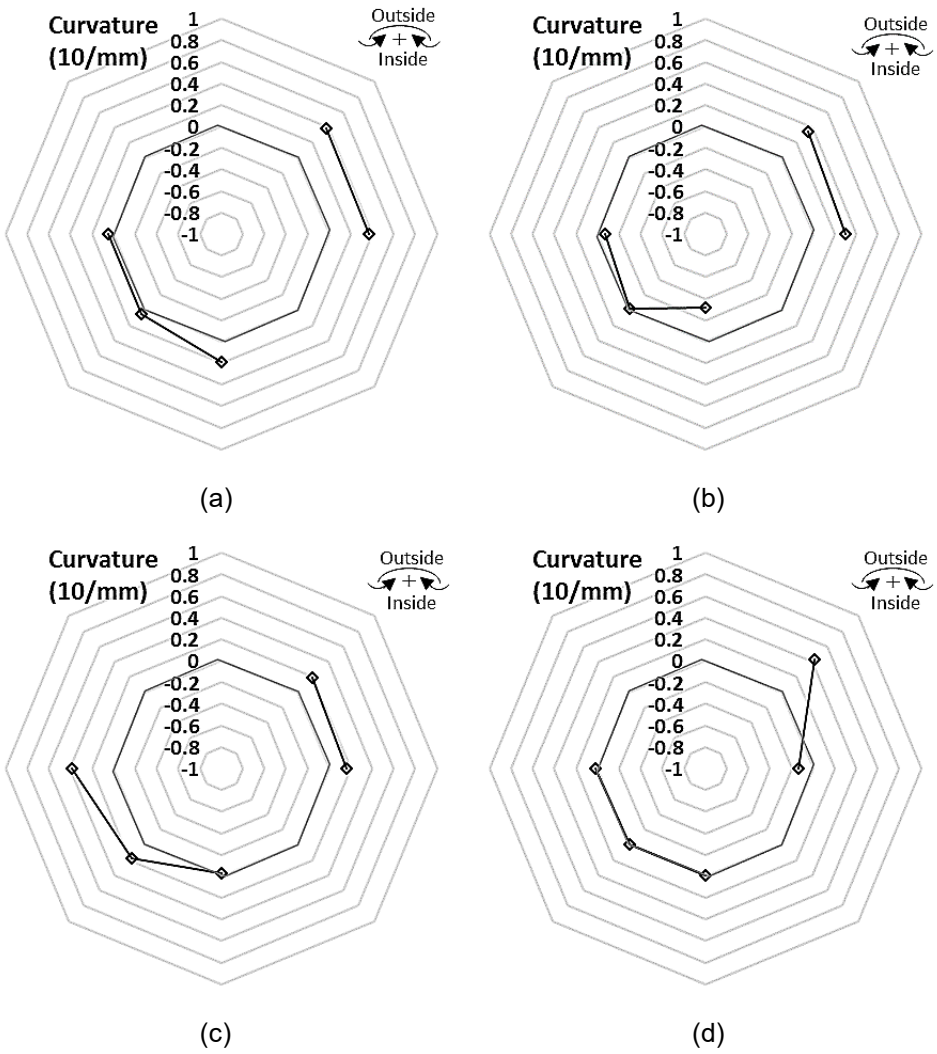

Figure 4.10: Curvature around the liner at the locations of Section 1: (a) after installing the liner; (b) after grouting; (c) at 7 days after grouting; and (d) at 28 days after grouting

4.3.3 Truck Loading Test

Traffic and truck loading tests have been commonly used to evaluate deformations of low-fill culverts under roadways (i.e., Han et al., 2013; Han et al., 2015). A loaded dump truck was used for the truck loading test in this study as shown in Figure 4.11. The truck consisted of three physical axles including a front steering axle with single tires and tandem axles with dual tires at the end. According to Han et al. (2018), this type of the loaded dump truck has an average total load of approximately 266 kN. Figure 4.11(b) shows the axle configuration, the contact area of the wheels, the distance between wheels, and the load on each axle. For each axle of this vehicle, the

load was determined based on Han et al. (2018). The load of the front steering axle (Axle 1) was 85 kN. The tandem axles were 4.57 m from the front axle and had a 90.4 kN load on each axle (Axles 2 and 3). Han et al. (2018) also developed a stress distribution program that can consider the type of pavement, the thicknesses of pavement layers, the elastic moduli of pavement layers, the types of design trucks, and the stress overlapping areas under a tandem axle load. This program is used to calculate the maximum distributed stresses induced by the tandem axles above the steel pipe. The calculated maximum distributed stresses using the load and resistance factor design (LRFD) method and the load factor design (LFD) methods were 35.7 and 25.9 kPa, respectively.

The responses of the un-rehabilitated and the rehabilitated steel pipes were monitored under truck loading. Since the corroded corrugated steel pipe was located before the T intersection, there was not enough space for the truck to be driven at a constant speed above the pavement. Therefore, the truck stopped for approximately one minute above the pipe for each axle loading. Three load combinations were obtained through truck loading by placing axles of the truck over Section 1 as shown in Figure 4.11(c). The location of Section 1 was marked with red spray paint on the surface to facilitate positioning of the truck wheels for each axle loading. All the axles were placed on the marks to create loading positions as shown in Figure 4.11(a) and (c).

The vertical diameter change of the unlined corroded steel pipe was measured using a DT located above a wheeled scissor jack as shown in Figure 4.12(a). The wheeled scissor jack was pushed inside the corroded steel pipe and positioned at the location of Section 1, and raised until the DT touched the crown of the steel pipe.

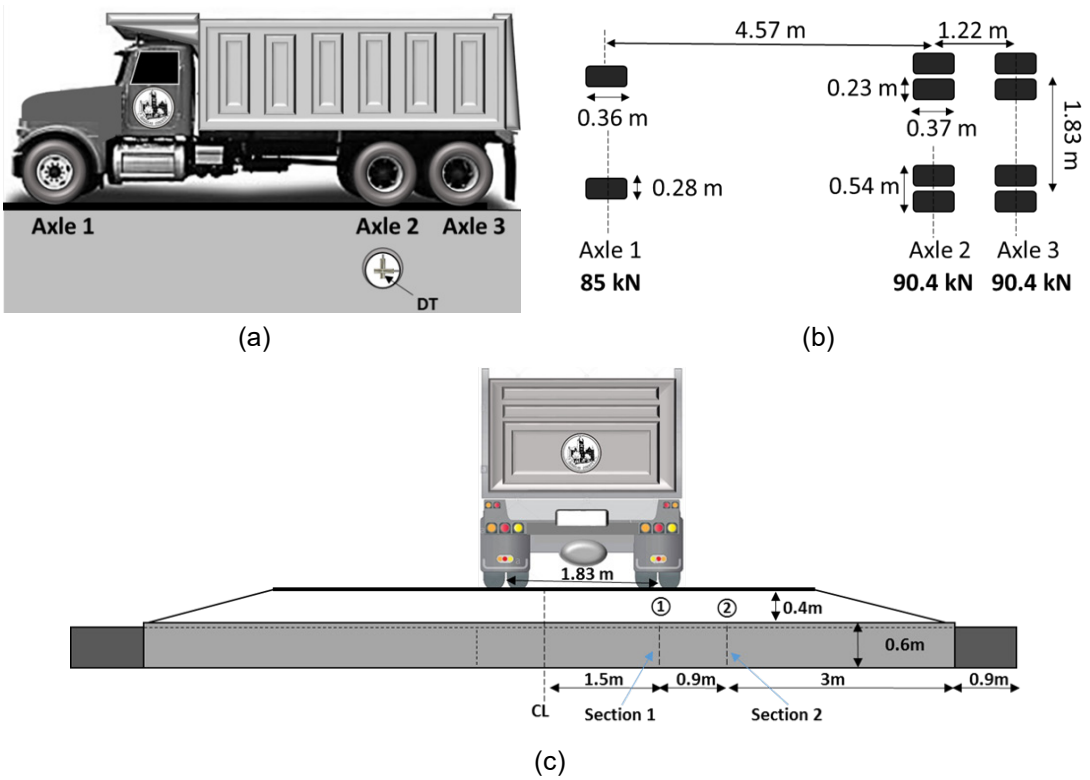

Figure 4.11: Truck loading test: (a) dump truck and axles; (b) axle configuration and load; and (c) cross-sections of the pipe and truck (not to scale)

Figure 4.13 shows the induced vertical and horizontal diameter changes of the steel pipe and the liner in Section 1 under wheel loading during several passes of the truck. The dotted line shows the vertical diameter change of the un-rehabilitated corroded steel pipe under three passes of the truck. The dashed and solid lines show the vertical and horizontal diameter changes of the liner under five passes of the truck at 7 and 28 days after grouting, respectively. Rahmaninezhad et al. (2019) found that in the sliplined steel pipes, the corrugated steel pipe, and the liner had a similar vertical diameter change under parallel-plate loading. Therefore, in this field study, it is assumed that after sliplining, the measured vertical diameter changes in the liner represented the vertical diameter changes of the steel pipe. Figure 4.13 shows that during truck loading, L1 decreased in the direction of the applied load while L2 increased. The average vertical diameter changes of the unlined steel pipe and the lined pipe before sliplining, at 7, and at 28 days after grouting under truck loading were -0.92, -0.20, and -0.17 mm, respectively. These results indicate that sliplining, at 7 and 28 days after grouting, reduced the vertical diameter changes of the

corroded steel pipe by approximately 78.2% and 81.5%, respectively. Rahmaninezhad et al. (2019) demonstrated that, in the sliplined pipes, the horizontal diameter change of the steel pipe was larger than the horizontal diameter change of the liner. Therefore, the horizontal diameter change of the liner could not represent the horizontal diameter change of the steel pipe. Figure 4.13 shows the average horizontal diameter changes of the liner at 7 and 28 days after grouting under truck loading were 0.19 and 0.26 mm, respectively.

Figure 4.14 shows the measured strains around the circumference of the liner at 7 days after grouting. The strains were induced by Axle 1 placed above the pavement at the location of Section 1. The approximate applied pressure by each wheel of Axle 1 was 422 kPa. The applied load via Axle 1 induced tensile strains on the inner face of the liner at the crown and right springline as shown in Figure 4.14(a). A higher tension on the inner face than the outer face of the liner at the right springline generated a negative curvature on that location in Section 1 as shown in Figure 4.15(a). Figure 4.14(b) and Figure 4.15(b) show that truck loading did not induce any significant strain and curvature on the liner in Section 2.

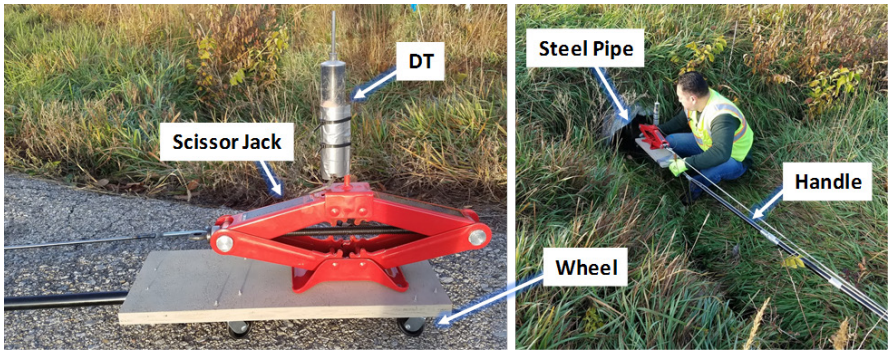

Figure 4.12: DT located above a wheeled scissor jack

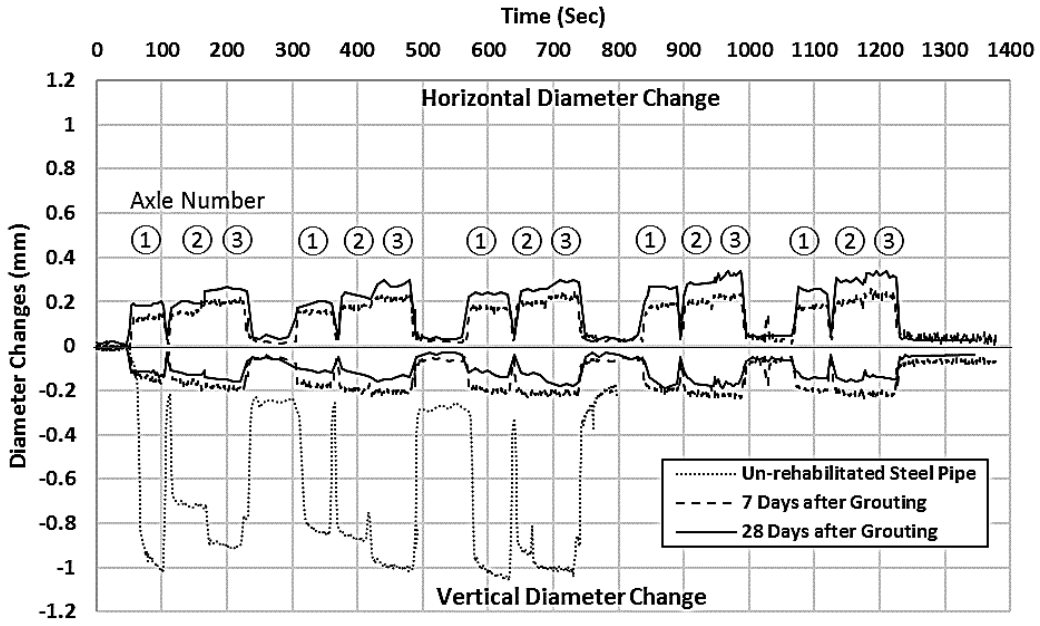

Figure 4.13: Vertical and horizontal diameter changes versus time at the location of Section 1

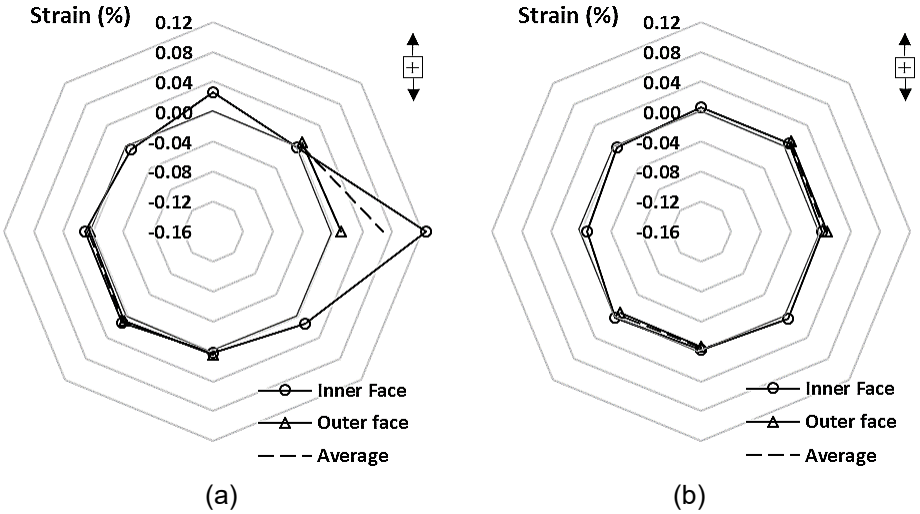

Figure 4.14: Induced inside and outside strains around the liner under Axle 1 load: (a) Section 1 and (b) Section 2

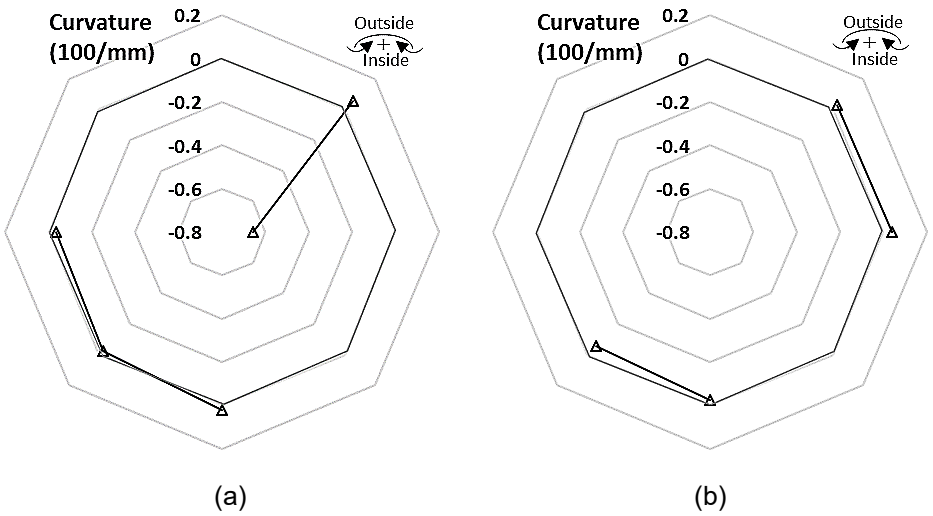

Figure 4.15: Induced curvatures around the liner under Axle 1 load: (a) Section 1 and (b) Section 2

4.3.4 Plate Loading Test

The plate loading test has been commonly used to evaluate subgrade soils and flexible pavement components for pavement design (i.e., Rahmaninezhad et al., 2009; Khatri, Han, Corey, Parsons, & Brennan, 2015; Mahgoub and El Naggar, 2018). Three in-place repetitive static plate loading tests in accordance to the ASTM D1195/D1195M-09 (2015) were conducted to evaluate the effect of sliplining on the settlement of the pavement surface due to loading. The loaded dump truck, which was utilized for the truck loading test, was used for the plate loading test on the pavement surface as shown in Figure 4.16. The vertical load was applied using a hydraulic jack with a maximum capacity of 12 tons. This jack was placed on a circular steel plate of 300 mm in diameter and 35 mm thick. The plate was placed directly above the surface of the asphalt pavement at the location of Section 1. The S-shape load cell was connected to the hydraulic jack to measure the applied load as shown in Figure 4.16. Two DTs were utilized to measure the vertical movement of the plate due to the applied load. The DTs were mounted on a reference beam, which was fixed on the I-beam section located at 2 m from the circular plate. After the test setup was complete and before the load was applied, the readings of the load cell and DTs were set to zero. The load was applied in nine load increments with approximately equal magnitude up to the desired maximum

load of 50 kN, (equal to the maximum capacity of the S-shape load cell). Finally, the load was released in one stage.

The average measured displacement from two DTs represented the settlement of the plate. Figure 4.17 shows the pressure-settlement curves of the plate. When the applied pressure was lower than 110 kPa, the pressure-settlement curves, before and after sliplining, were similar. However, after 110 kPa, the pavement before sliplining had larger settlement than the pavement at 7 and 28 days after grouting. Then, after 550 kPa, the pavement at 7 days after grouting behaved similarly to that without sliplining again. Under the applied pressure of 780 kPa, the settlement values of the plate on the pavement before sliplining, at 7 days, and 28 days after grouting were approximately 1.6, 1.5, and 1.1 mm, respectively. In other words, sliplining and grouting reduced the settlement of the pavement at 7 and 28 days after grouting by 6% and 31%, respectively, as compared with that before sliplining. In all tests, the permanent settlement of the pavement after unloading was approximately 0.8 mm.

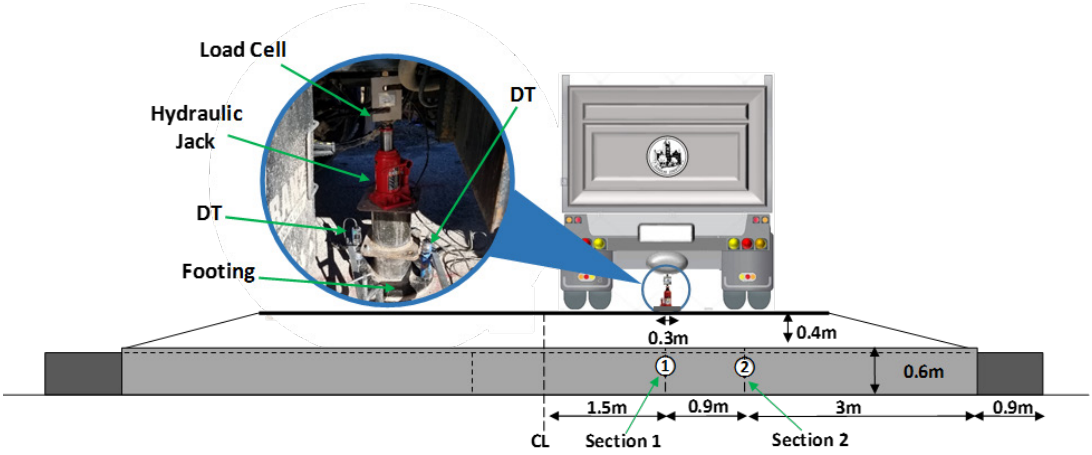

Figure 4.16: Plate loading test setup (not to scale)

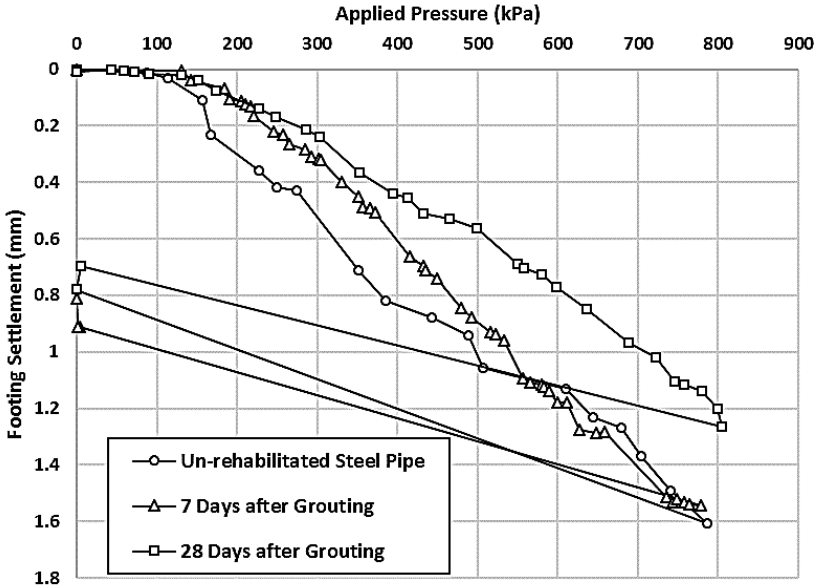

Figure 4.17: Pressure-settlement curves of the plate

Figure 4.18 shows the applied pressures versus the diameter changes that were measured by the DTs mounted inside the steel pipe and liner at the location of Section 1. Under the applied pressure, the distance between the crown and the invert decreased in the direction of the applied pressure. However, the distance between the springlines increased. The vertical diameter changes of the steel pipe before sliplining were larger than that after sliplining. In other words, the steel pipe after sliplining behaved stiffer than that before sliplining. For instance, when the applied pressure was 780 kPa, the vertical diameter changes of the steel pipe before sliplining, at 7 days, and 28 days after grouting, were approximately 1.15, 0.15, and 0.12 mm, respectively. The sliplining after 7 and 28 days reduced the vertical diameter changes of the corroded steel pipes by 87% and 90%, respectively, as compared with that before sliplining.

Unfortunately, the wheeled scissor jack, as shown in Figure 4.12, did not measure the horizontal diameter change of the un-rehabilitated corroded steel pipe. Figure 4.18 shows that at 7 days after grouting, the vertical and horizontal diameter changes were almost equal with opposite signs. However, at 28 days after grouting, the horizontal diameter changes were larger than the vertical diameter changes at the same applied load, which were probably related to water freezing within the surrounding grout.

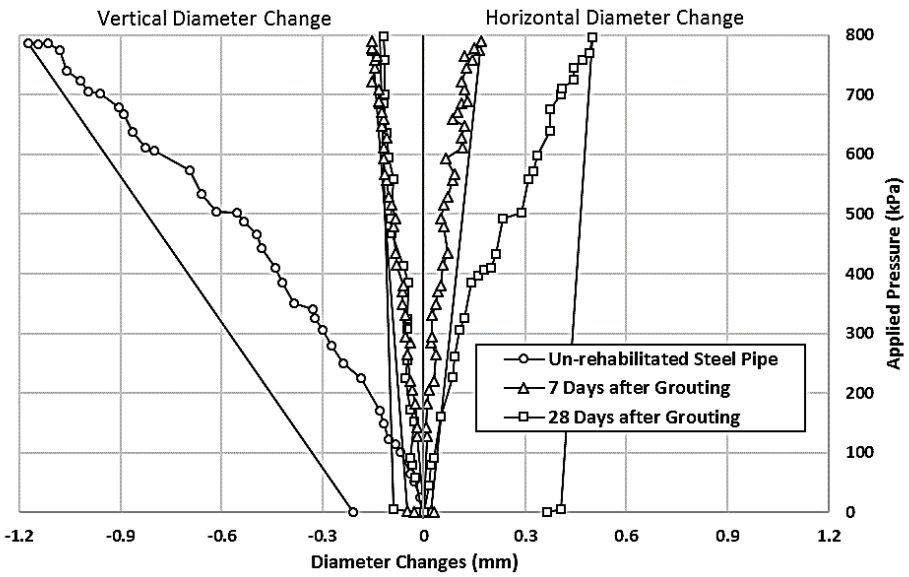

Figure 4.18: Applied pressure versus vertical and horizontal pipe diameter changes

Chapter 5. Behavior of Buried Sliplined Corrugated Steel Pipes Subjected to Footing Loading in Laboratory

5.1 Introduction

This chapter contains an evaluation of the effect of sliplining on the behavior of buried corroded corrugated steel pipes in sand under footing loading in a geotechnical test box, including: (1) load-carrying capacity and stiffness of the pipe; (2) vertical and horizontal diameter changes of the pipes; and (3) vertical and lateral earth pressures around the pipe. Two series of the surface footing loading tests were conducted on the unlined and sliplined buried corrugated steel pipes with different degrees of corrosion. After the surface footing loading tests were conducted, the rehabilitated steel pipes were exhumed from the test box. Then, a series of parallel plate loading tests were carried out on the exhumed rehabilitated pipes using a universal testing machine. The results of the parallel plate loading tests include: (1) load-carrying capacity and stiffness of the sliplined pipes, and (2) vertical and horizontal diameter changes of the sliplined pipes.

5.2 Footing Loading Tests

5.2.1 Test Apparatus

Six model tests were carried out to investigate the effect of sliplining on the behavior of the corrugated steel pipes with different degrees of corrosion subjected to static loading on a rigid footing under a plane-strain condition. The test box was designed to accommodate a plane-strain condition with interior dimensions of 1.76 m long, 0.46 m wide, and 1.50 m high. This box was made of three sides of plywood and a Plexiglas plate on the front side to allow visual observation of soil deformations during the test. Steel square tubes were installed all around the box to minimize lateral deflections of box walls. In addition, the Plexiglas plate was stiffened by four sections of steel angle along the front side. A double layer of thick plastic sheet covered three sides of the test box made of plywood. The layer in contact with the box wall was fixed, while the layer in contact with the soil was free to move with minimum frictional resistance from the box walls. Plastic sheets or lubricant for boundary treatment have been successfully used in many experimental studies (e.g., Zarnani et al., 2011; Ahmed, 2016; Hong et al., 2016; Kakrasul et al., 2016). The distance from each side of the steel pipe to the box wall was 0.73 m, which is twice the

width of the buried structure as recommended by Bloomquist et al. (2009). On the top of the fill, a footing load was applied using a hydraulic jack attached to a rigid steel footing that was centered above the steel pipe as shown in Figure 5.1. The hydraulic jack had a load capacity of 25 tons.

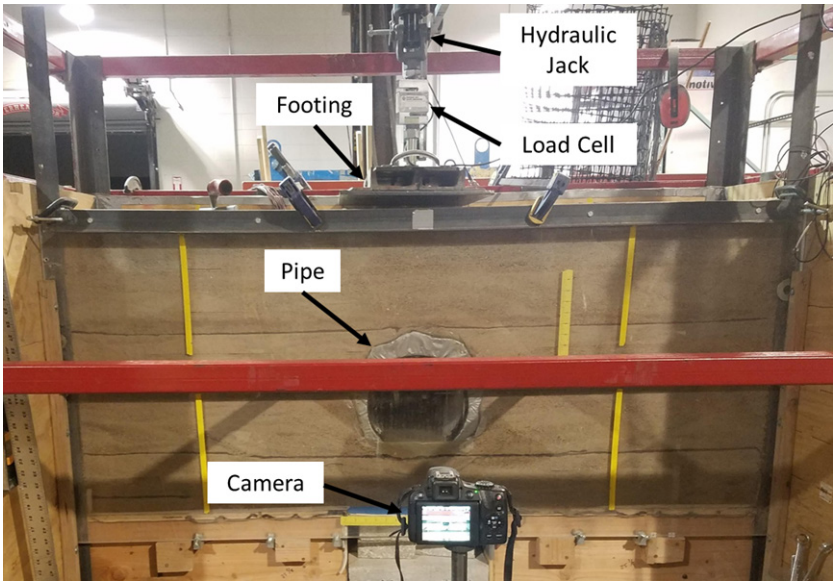

Figure 5.1: Setup of a footing loading test on one sliplined buried pipe

The rigid strip footing was made of a 25-mm-thick steel plate. The steel plate was reinforced by two steel profiles to minimize its bending under loading. The footing was 360 mm wide and 455 mm long. To ensure a plane-strain condition, the length of the footing was equal to the internal width of the test box. Figure 5.1 shows the strip footing at the center of the text box.

5.2.2 Backfill

A dry poorly-graded Kansas River sand was used in this study as the backfill. The mean grain size (D_{50}) was 0.56 mm. The uniformity coefficient (C_u) and the coefficient of curvature (C_c) of the sand were 3.18 and 0.93, respectively. The maximum and minimum dry unit weights of the sand were 18.9 and 16 kN/m^3, respectively. Rahmaninezhad et al. (2009) discussed the effect of compaction on the reinforced sand in reduced-scale models. A standard direct shear test (ASTM D3080, 2011) was used to determine the friction angle of the sand compacted at 70% relative density. The measured peak friction angle of the sand was 37°.

5.2.3 Steel Pipes and Liners

The same corrugated steel pipes and liners used in parallel-plate loading tests as reported in Chapter 3 were used in the footing loading tests. The corrugated steel pipe sections had a nominal inside diameter of 300 mm and a length of 455 mm. They had a nominal wall thickness of 2 mm with a corrugation height of 15 mm and a corrugation length of 70 mm. The average cutout areas along the invert of two steel pipes were 50% and 90% to represent 50% and 90% degree of corrosion, respectively, as shown in Figure 3.3. The PVC liners had an inside diameter of 254 mm, a wall thickness of 3 mm, and a length of 455 mm. Figure 3.4 shows the applied load versus diameter change for the PVC liner, indicating a linear load-diameter change relationship.

5.2.4 Grout

The grout used in the field study as reported in Chapter 4 was used for sliplining in these model tests. This low-viscosity grout was able to flow through the space between the steel pipe and the liner easily. The mix of this grout included 254 kg/m^3 cement, 384 kg/m^3 fly ash, and 492 kg/m^3. As discussed in Chapter 4, the unconfined compression tests were conducted on the grout specimens using the ASTM C39/C39M (2004) standard to determine their average seven-day compressive strength of 2.7 MPa.

5.2.5 Measurements

The applied load was measured using an S-shape load cell with a load capacity of 22.3 kN mounted above the footing. A pressure gauge was used to control the hydraulic pressure applied to the footing. The settlement of the footing, and the vertical and horizontal diameter changes of the liner were measured using two types of DTs with displacement limits of 100 mm and 50 mm, respectively. Pressure cells were used to measure vertical and lateral earth pressures as shown in Figure 5.2.

Figure 5.2: Earth pressure cells

5.2.6 Test Configuration

Figure 5.3 shows the cross-section of the test setup including the locations of the footing, the load cell, the displacement transducers, and the pressure cells. The pipe was buried at a depth of 300 mm (from the surface to the top of the pipe) for each model. A rigid plate was used to apply the load on the surface of the backfill. Two series of tests were conducted in this part of the study. The first series of tests, Series A, was conducted on the simulated corroded steel pipes without a liner as shown in Figure 5.3(a). In these tests, the steel pipes had 0%, 50%, and 90% cutout, where the 0% cutout represents an intact steel pipe. In the second series of tests, Series B, three tests were carried out on sliplined steel pipes with 0%, 50%, and 90% cutout as shown in Figure 5.3(b). In these tests, the liners were placed on the invert of the steel pipes. After each footing plate loading test, the pipe was exhumed from the soil for a parallel-plate loading test.

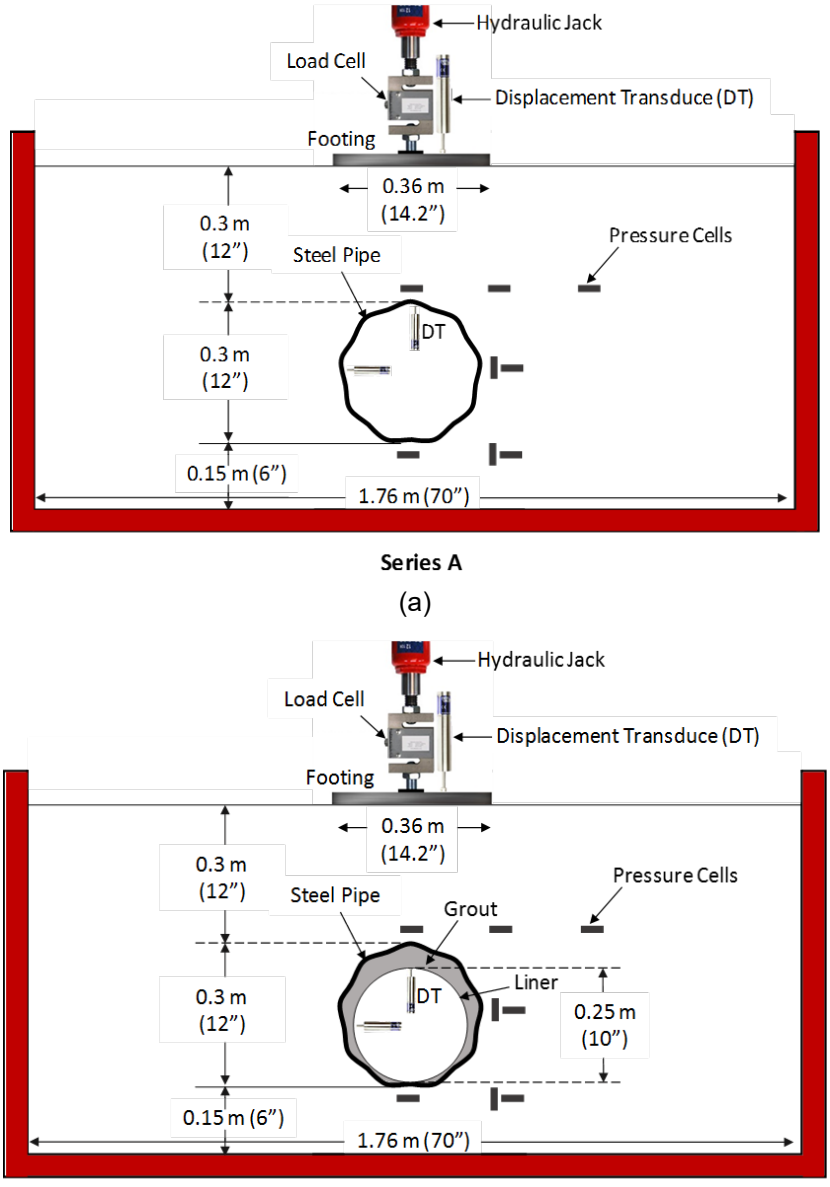

Figure 5.3: Test configurations: (a) Series A, unlined steel pipe and (b) Series B, sliplined steel pipe

5.2.7 Model Preparation

Each model was constructed in four lifts with a lift thickness of 150 mm in addition to a 150-mm-thick bedding layer underneath the pipe. After placement of each lift of the sand, it was compacted to a relative density of 75% using a mass-volume control method. Before placement of the steel pipe, the PVC liner was inserted into the pipe. Both ends of the steel pipe were sealed

using a foam to minimize the leakage of grout. After placement of the pipe, sand was placed around the pipe up to its springlines and the pressure cells were installed. Figure 5.4 shows the steel pipe, the liner, and two pressure cells. Additional sand was placed up to the pipe crown. To pour the grout into the annulus between the steel pipe and the liner, a 40-mm-diameter hole was drilled into the crown of the steel pipe and a PVC pipe of 40 mm in diameter and 0.4 m long was connected to the hole as a drop tube. After the installation of the tube, the last two lifts of sand were placed and compacted above the crown up to the surface.

After the model construction, the grouting process was started and completed in two stages to mitigate the buoyant force of the grout. The first stage of grouting reached the haunch level while the second stage of grouting filled the rest of the annulus. Figure 5.5 shows pouring of the grout into the annulus through a drop tube. During grouting, some grout leaked out through the cutout area and pipe ends into the bedding sand. The dotted line in Figure 5.6 shows the area where the grout leaked in the bedding sand. The volumes of the grout used for the pipes with 0%, 50%, and 90% cutout were 0.011, 0.013, and 0.015 m^3. Upon the completion of two grouting stages, the model was left for seven days for the grout in the annulus to set.

5.2.8 Footing Loading

At seven days after grouting, the soil surface was subjected to a static footing load. The load was applied in equal increments up to 140 kPa and then unloaded to zero. At each load increment, the plate settlement, the pipe deformations, and the pressures in the soil were measured by the sensors. These data were used to evaluate the performance of unlined and lined pipes at different degrees of cutout and the benefit of sliplining the pipes buried in the soil. After the footing loading test, the pipe was exhumed from the soil for the parallel-plate loading test.

Figure 5.4: Placed steel pipe and liner

Figure 5.5: Pouring grout into the annulus through a drop tube

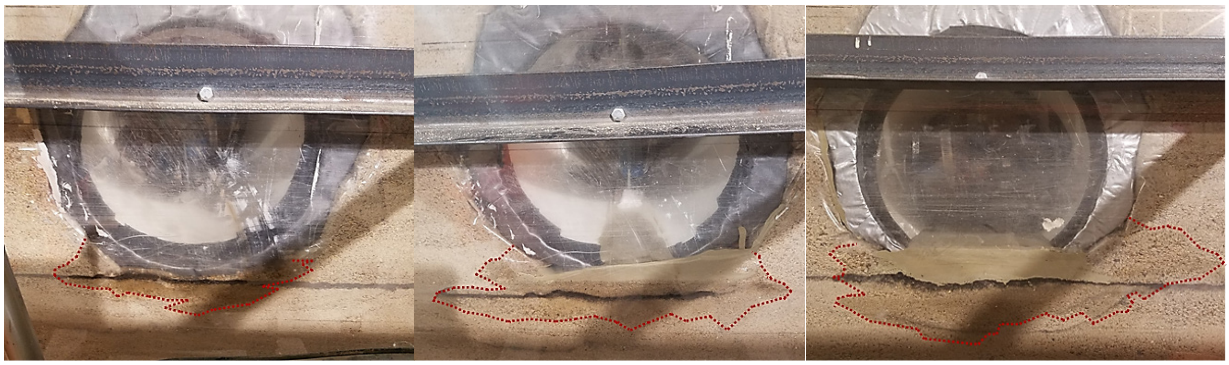

(a) (b) (c)

Figure 5.6: Leaked grout: (a) 0% cutout, (b) 50% cutout, and (c) 90% cutout

5.3 Parallel-Plate Loading Tests

5.3.1 Test Apparatus

The universal testing machine with a load capacity of 534 kN was used to apply vertical loads on the exhumed rehabilitated steel pipes.

5.3.2 Measurements

The applied load was measured using an S-shape load cell with a load capacity of 40 kN. The vertical and horizontal diameter changes of the steel pipes and the liners were measured using two types of displacement transducers (DTs) with displacement limits of 100 mm and 50 mm.

5.3.3 Test Configuration

Figure 5.7 shows the schematic cross-section of the test setup including the locations of the load cell and displacement transducers. On the top of the pipe, a rigid plate was used to apply the load to the pipe. A series of tests were conducted on the exhumed rehabilitated steel pipes. The exhumed steel pipes had 0%, 50%, and 90% cutout. Moreover, the liners in these tests were placed on the invert of the steel pipes.

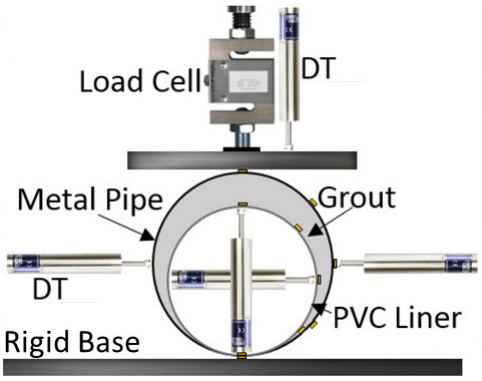

Figure 5.7: Test configurations

5.4 Test Results and Discussion

5.4.1 Footing Loading Tests

5.4.1.1 Footing Settlement

The settlement of the footing at the center after each applied pressure was measured by the DT. Figure 5.8 shows the pressure-settlement curves of the footing on the backfill with the unlined steel pipes with 0%, 50%, and 90% cutout. The results show that the models with the pipes having 50% and 90% cutout had larger settlements than the model with the steel pipe without any cutout (0% cutout). When the applied pressure was lower than 122 kPa, the model with the pipe with 90% cutout behaved stiffer than that with 50% cutout. As discussed in Chapter 3, this phenomenon resulted from the fact the pipe with 90% cutout behaved like an arch. However, after 122 kPa, the model with the pipe with 50% cutout had smaller settlement than that with 90% cutout. Under the applied pressure of 140 kPa, the footing settlement in the models with the unlined steel pipes with 0%, 50%, and 90% cutout were 19, 33, and 35 mm, respectively.

Figure 5.9 shows the pressure-settlement curves of the footing in the models with the sliplined steel pipes with 0%, 50%, and 90% cutout. The result shows that the model with the sliplined steel pipe with a lower degree of cutout had a lower load capacity than that with a higher degree of the cutout. This phenomenon resulted from the grout that leaked out into the bedding sand. The leaked grout made the bedding sand under the pipes with 90% and 50% cutout stronger than that under the pipe with 0% cutout. Moreover, because of the arch behavior of the pipe with 90% cutout, the model with this pipe behaved stiffer than that with the steel pipe with 50% cutout.

5.4.1.2 Diameter Changes

Figures 5.10 and 5.11 show the applied load versus diameter change curves for the steel pipes. During loading, the distance between the crown and the invert decreased in the direction of the applied load. However, the distance between the springlines increased. Figure 5.10 shows that the unlined steel pipe with 0% cutout had a higher load capacity than the pipes with 50% and 90% cutout for the Series A tests. The unlined steel pipes had outside vertical and horizontal diameter changes that were of approximately equal magnitude but with opposite signs. When the applied

pressure was lower than 115 kPa, the steel pipe with 90% cutout had less vertical diameter change than the pipe with 50% cutout. However, above 115 kPa, the pipe with 50% cutout had smaller vertical diameter changes than the pipe with 90% cutout while the steel pipe with 90% cutout had smaller horizontal diameter changes than the pipe with 50% cutout. As discussed in Chapter 3, this phenomenon resulted from the fact that the pipe with 90% cutout behaved like an arch with a flat base.

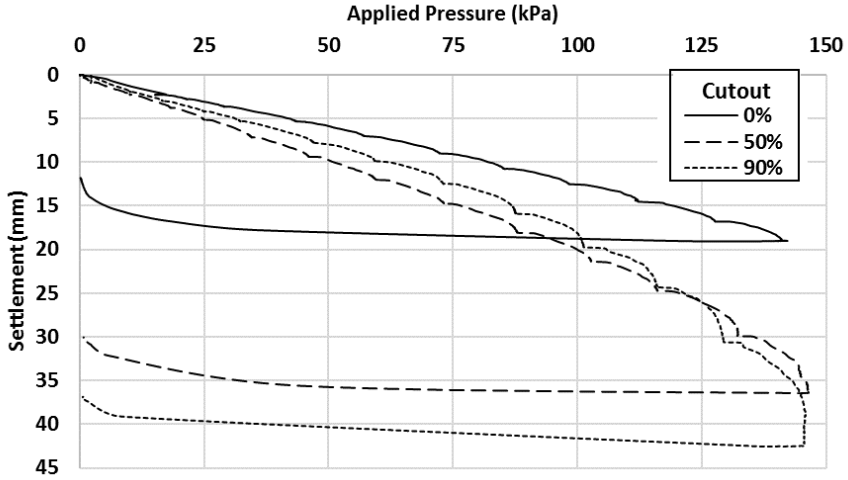

Figure 5.8: Pressure-settlement curves of the footings for the models with the unlined steel pipes in test Series A

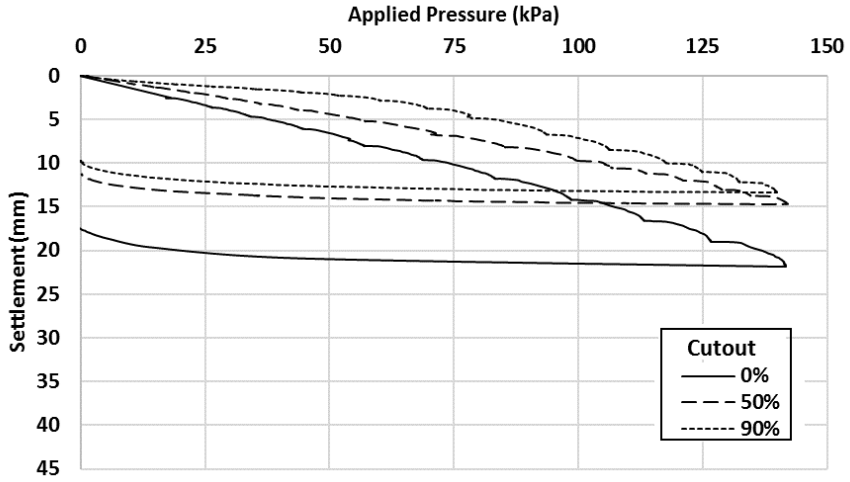

Figure 5.9: Pressure-settlement curves of the footings for the models with the sliplined steel pipes in test Series B

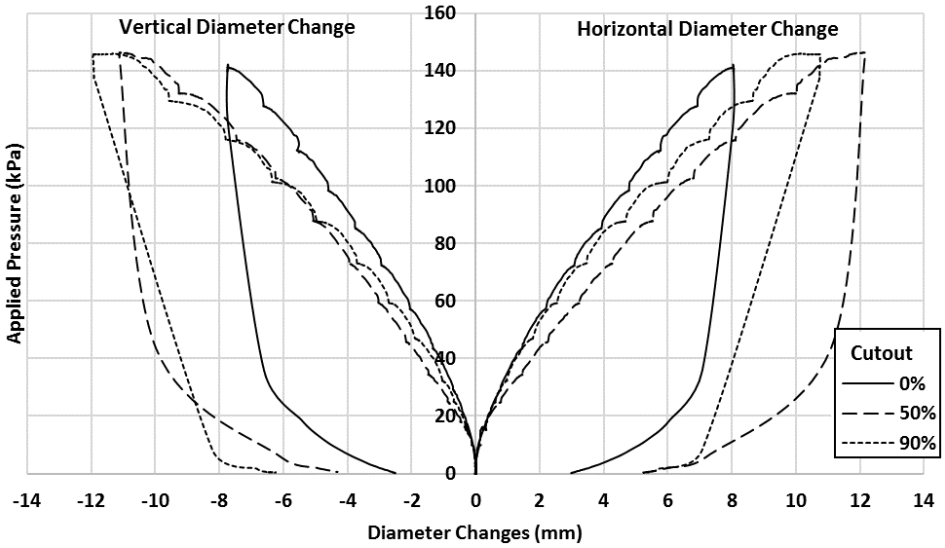

Figure 5.10: Applied load versus vertical and horizontal diameter changes for test Series A

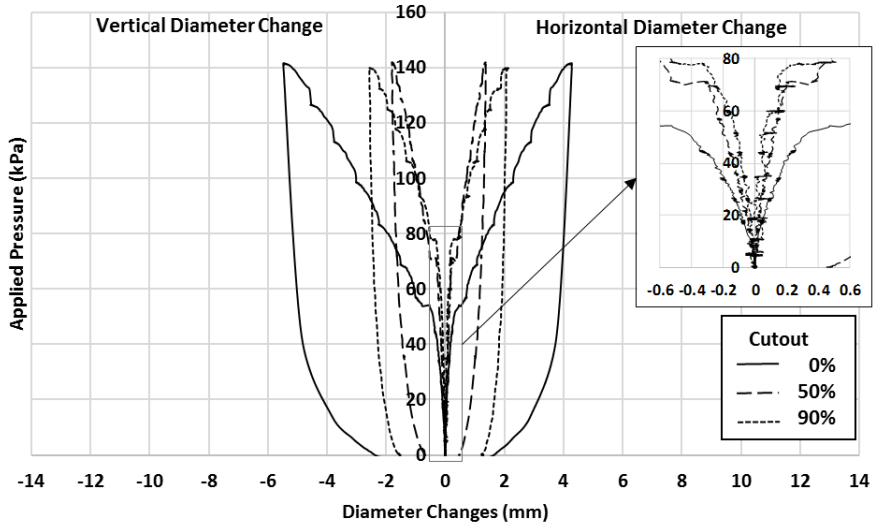

Figure 5.11: Applied load versus vertical and horizontal diameter changes for test Series B

Figure 5.11 shows the sliplined steel pipes in the Series B tests. The results indicate that the sliplined steel pipe with 50% cutout had a higher load capacity than the pipes with 0% and 90% cutout. The sliplined steel pipes had larger vertical diameter changes than horizontal diameter changes at the same applied load. When the applied pressure was lower than 90 kPa, the steel pipe with 90% cutout behaved stiffer than the pipe with 50% cutout. However, above 90 kPa, the pipe with 50% cutout behaved stiffer than the pipe with 90% cutout. Figures 5.10 and 5.11 indicate that

sliplining reduced the diameter changes of the unlined steel pipes. For instance, under the applied pressure of 130 kPa, the vertical diameter changes of the steel pipes with 0%, 50%, and 90% cutout after sliplining were 1.5, 5.6, and 5.3 times, respectively—less than those before sliplining.

5.4.1.3 Vertical Pressure

Figure 5.12 presents the vertical earth pressures induced by footing loading around the unlined steel pipes for test Series A. The locations of the earth pressure cells (EPCs) are shown in this figure. It should be noted that the measured earth pressures are the additional pressures induced by footing loading and do not include the pressure due to the soil self-weight. The measured vertical earth pressures generally increased with the increase of the applied footing pressure for the unlined steel pipes. These results indicate that in the models with the unlined steel pipes, EPC6 measured higher pressures than EPC7 at the same applied pressure. The measured pressures from EPC1 and EPC6, which were placed under and above the unlined steel pipe with 0% cutout, respectively, were higher than those with 50% and 90% cutout. Moreover, in these tests, the measured pressure from EPC6 was higher than that from EPC1. For example, in the model with the pipe having 0% cutout, the measured pressure from EPC6 was approximately three times that from EPC1. However, at the same applied pressure, the measured pressures from EPC2, EPC5, and EPC7 were approximately equal. This phenomenon resulted from the fact that the model with the unlined steel pipe having 0% cutout had higher stiffness than those having 50% and 90% cutout as shown in Figure 5.8. Since some segments were cut out along the invert of the steel pipes with 50% and 90% of the material removed to simulate corrosion, the measured pressure from EPC1 was lower than that from EPC2. However, in the model with the unlined steel pipe with 0% cutout, the measured pressure from EPC1 was higher than that from EPC2.

Figure 5.13 shows the vertical earth pressures induced by footing loading around the sliplined steel pipes for the Series B tests. The results indicate that EPC6 in the backfill with the sliplined steel pipes measured a higher pressure than EPC7 at the same applied pressure. In the model with the sliplined steel pipe having 0% cutout, the measured pressures from EPC1 and EPC6 were approximately equal, as shown in Figure 5.13(a). However, in the models with the sliplined steel pipe having 50% and 90% cutout, EPC6 measured a higher pressure than EPC1 at the same

applied pressure. In the models with the sliplined steel pipe having 90% cutout, Figure 5.13(c) shows a reduction on the measured pressure from EPC1 when the applied pressure was 78 kPa. At the same applied pressure, the measured pressures from EPC2, EPC5, and EPC7 were approximately equal.

5.4.1.4 Lateral Pressure

Figure 5.14 shows the lateral earth pressures induced by footing loading around the unlined steel pipes for test Series A. The results indicate that the measured lateral pressures in the model with the unlined steel pipe having 0% cutout were higher than those with 50% and 90% cutout. In the model with the unlined steel pipe having 0% cutout, when the applied pressure was lower than 69 kPa, the measured pressures from EPC3 were lower than those from EPC4 as shown in Figure 5.14(a). However, when the applied pressure was higher than 69 kPa, EPC3 measured higher pressures than EPC4. Moreover, in the model with the unlined steel pipes having 50% and 90% cutout, the measured pressures from EPC4 were lower than those from EPC3.

Figure 5.15 shows the lateral earth pressures induced by footing loading around the sliplined steel pipes for test Series B. The results show that regardless of the percentage of the cutout, the measured lateral pressures from EPC3 were higher than those from EPC4. The measured lateral pressures from EPC3 in the models with the sliplined pipes having 0% and 90% cutout and under the same applied pressure were approximately equal, as shown in Figures 5.15(a) and (b). However, the measured pressures from EPC4 in the model with the sliplined pipe having 0% cutout were higher than those having 50% cutout. In the model with the unlined steel pipe having 90% cutout, when the applied pressure was lower than 56 kPa, the measured pressures from EPC3 and EPC4 were approximately equal, as shown in Figure 5.15(c). However, when the applied pressure was higher than 56 kPa, EPC3 measured higher pressures than EPC4. Moreover, in the model with the sliplined steel pipe having 90% cutout, the measured pressures from EPC4 were lower than those in the model with the sliplined steel pipe having 50% cutout.

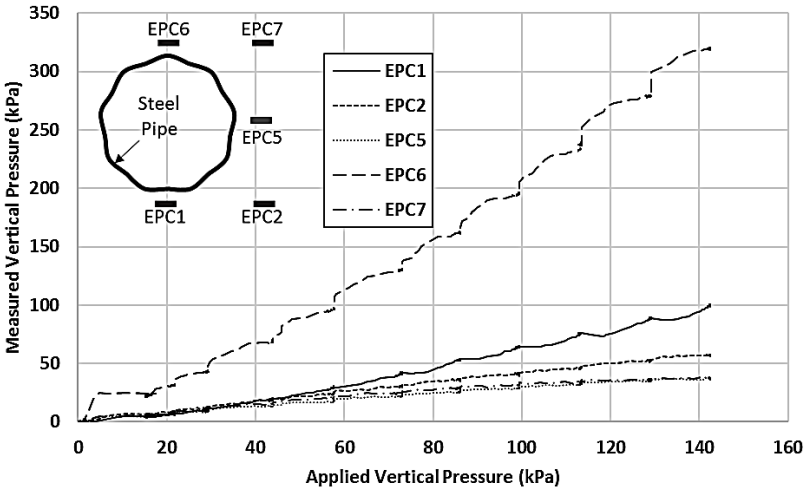

(a)

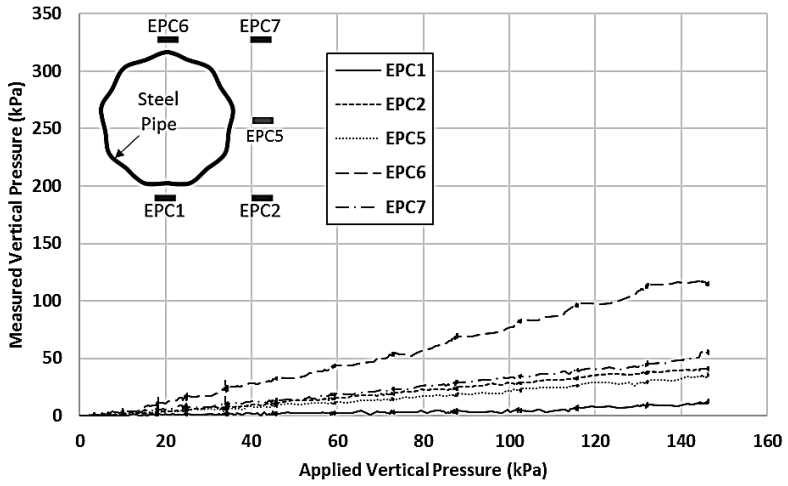

(b)

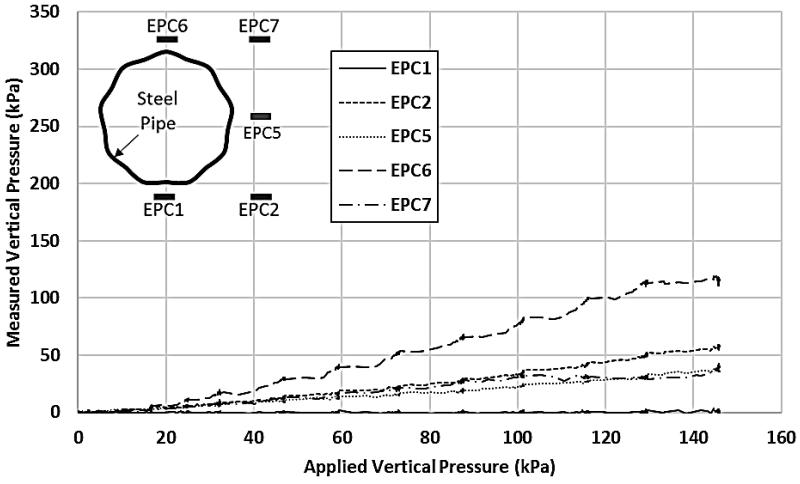

(c)

Figure 5.12: Measured vertical pressures around the unlined pipe in test Series A with: (a) 0%; (b) 50%; and (c) 90% cutout

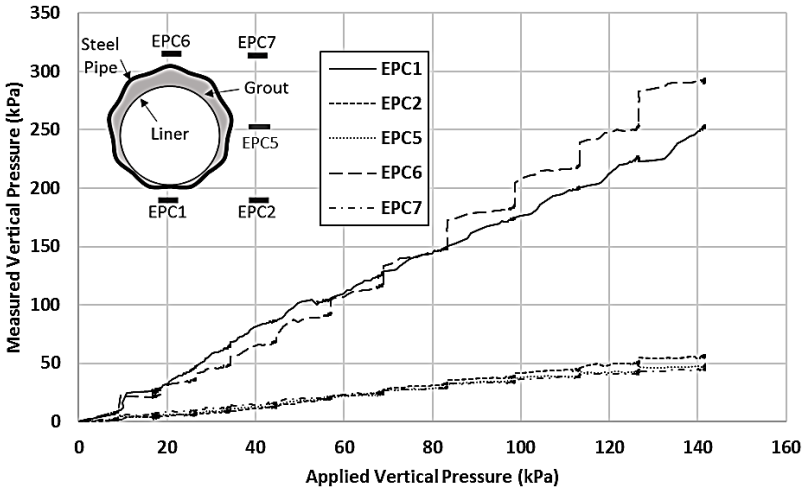

(a)

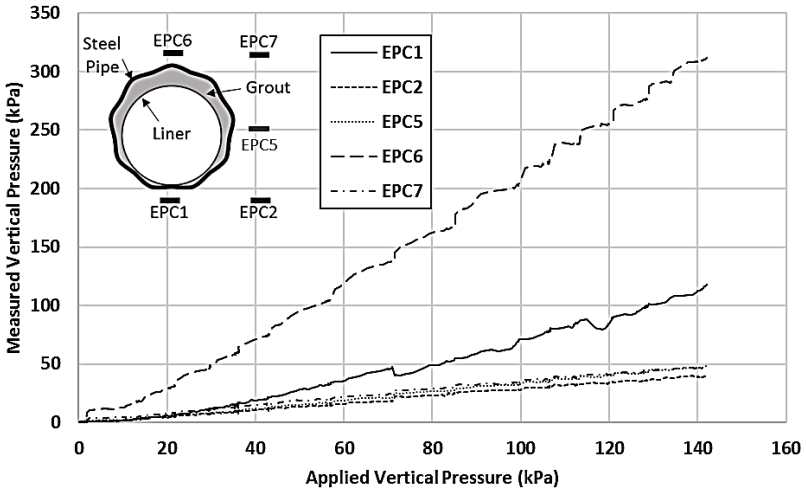

(b)

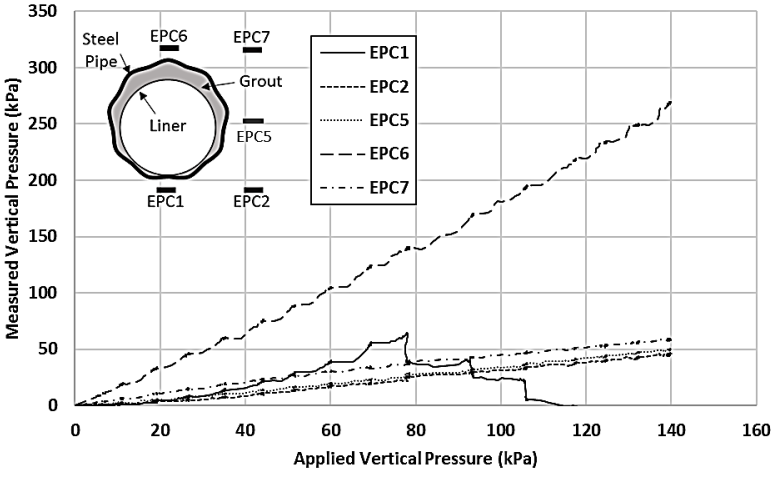

(c)

Figure 5.13: Measured vertical pressures around the sliplined pipes in test Series B with: (a) 0%; (b) 50%; and (c) 90% cutout

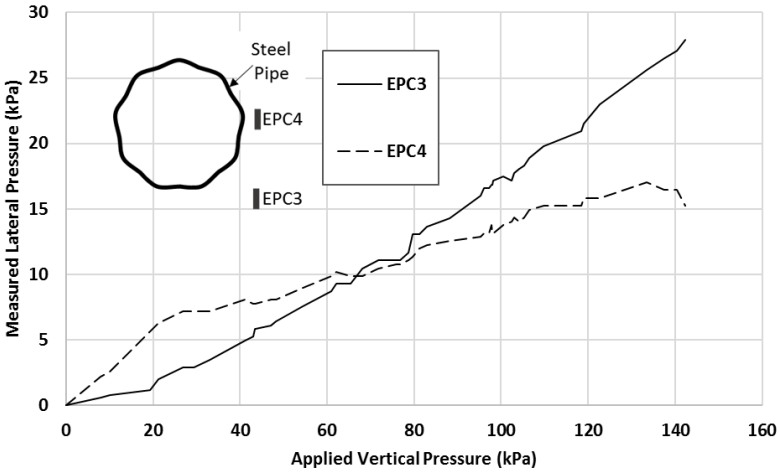

(a)

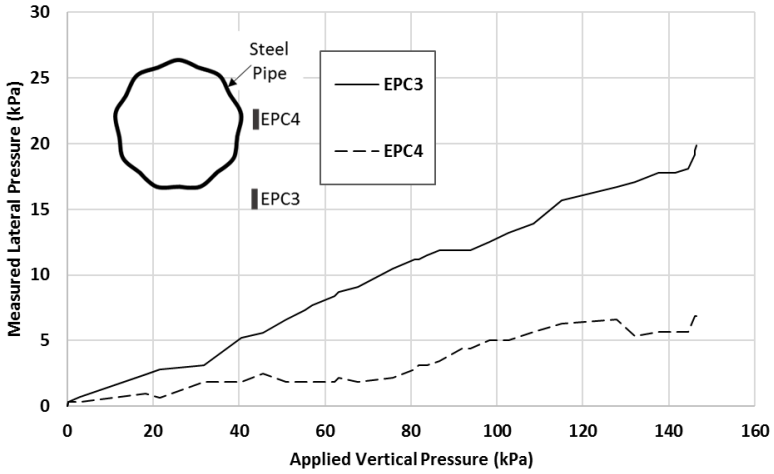

(b)

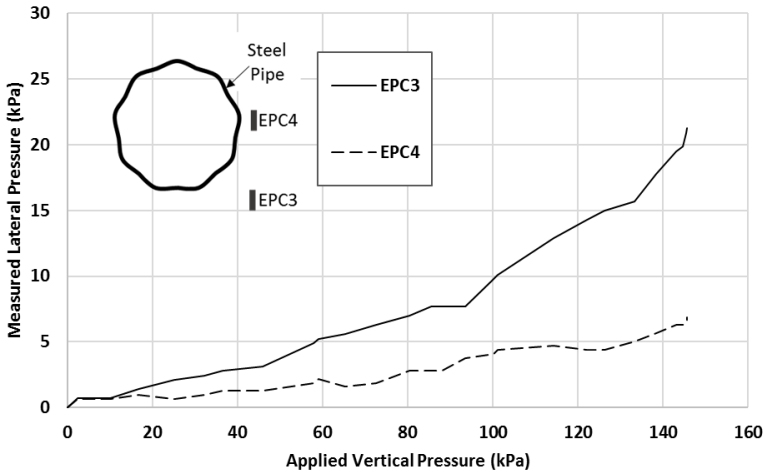

(c)

Figure 5.14: Measured lateral pressures around the unlined pipes in test Series A with: (a) 0%; (b) 50%; and (c) 90% cutout

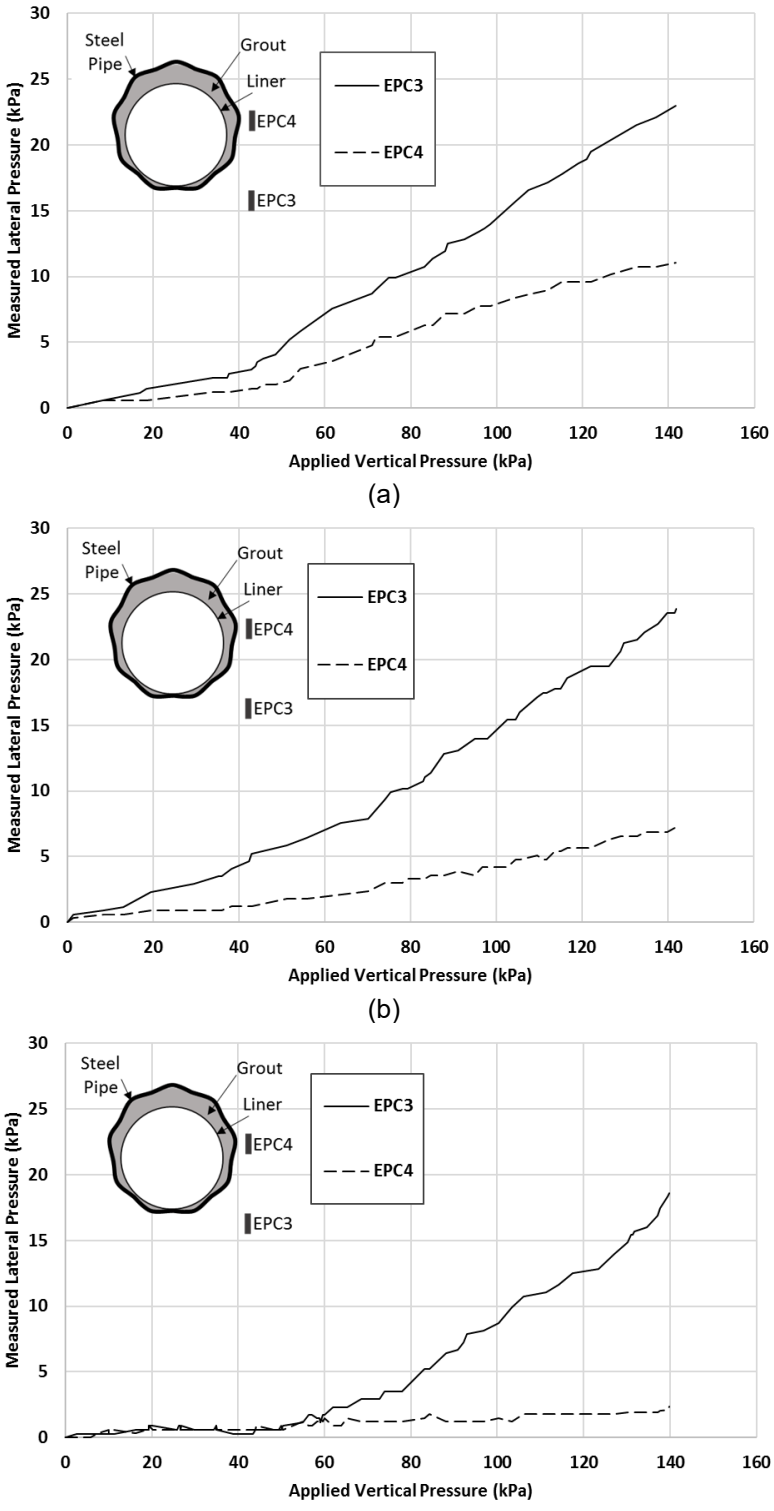

Figure 5.15: Measured lateral pressures around the sliplined pipes in test Series B with: (a) 0%; (b) 50%; and (c) 90% cutout

5.4.2 Parallel Plate Loading Tests

Figure 5.16 shows the applied load versus the vertical and horizontal outside diameter changes of the exhumed pipes that were measured by DTs installed outside the sliplined pipes. The results indicate that the sliplined pipes with 50% and 90% cutout behaved stiffer than the pipe with 0% cutout. Also, the vertical diameter changes of the sliplined pipes with 50% and 90% cutout were similar. However, the sliplined pipe with 50% cutout had smaller horizontal diameter changes than that with 90% cutout at the same applied load. The sliplined steel pipes with 0% and 50% cutout had vertical outside diameter changes of larger magnitude and opposite sign than the horizontal diameter changes. However, the pipe with 90% cutout had smaller vertical outside diameter changes than horizontal outside diameter changes. Figure 5.16 indicates that sliplining increased the load-carrying capacity of the unlined steel pipes. For instance, at 5% vertical diameter change, the load-carrying capacities of the steel pipes with 0%, 50%, and 90% cutout were increased by 1.4, 2.9, and 2.6 times, respectively.

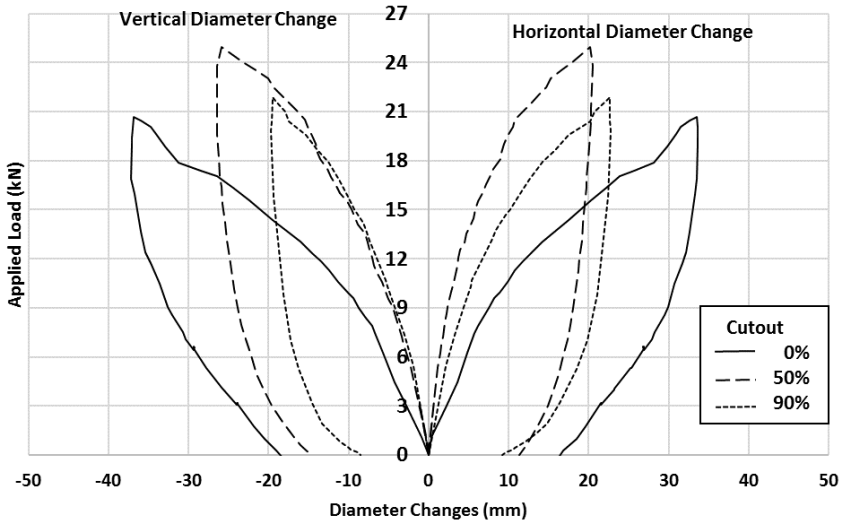

Figure 5.16: Applied load versus vertical and horizontal outside diameter changes

Chapter 6: Conclusions and Recommendations

6.1 Conclusions

This research project included three experimental studies: (1) parallel-plate loading tests of unlined and sliplined steel pipes with different degrees of corrosion (simulated by cutout) in air; (2) field truck and plate loading tests of corroded steel pipes before and after sliplining; and (3) footing loading tests on unlined and sliplined steel pipes with different degrees of corrosion in soil and parallel-plate loading tests of exhumed pipes in air. The following conclusions can be made from these three studies:

1. Parallel-plate loading tests in air:
    a. The sliplined steel pipes with 0%, 50%, and 90% cutout under vertical loading had average vertical to horizontal diameter change ratios of 0.98, 1.54, and 1.91, respectively, which were higher than those for the unlined steel pipes (i.e., 0.94, 1.12, and 1.03, respectively).
    b. Under the higher applied load, the unlined steel pipe with 90% cutout behaved stiffer than the unlined pipe with 50% cutout because the pipe with 90% cutout behaved as an arch.
    c. The sliplined steel pipe with a lower degree of corrosion had a higher load-carrying capacity than that with a higher degree of corrosion.
    d. The degree of corrosion and the location of the liner had an effect on the load-carrying capacity of the grout in the sliplined pipe. The grout carried a higher load when the liner was placed at the center than that when the liner was placed on the invert.
    e. Grout in the sliplined steel pipe with 0% cutout carried more load than the grout in the steel pipe with 50% cutout.
    f. When the unlined and sliplined steel pipes were subjected to vertical loading, negative strains were observed at the crown and invert of the steel pipes while the positive strains were localized at the springlines of these pipes.

g. The unlined steel pipes with 0% and 50% cutout had significant bending moments developing in the springline region and at the crown, respectively. However, the unlined steel pipe with 90% cutout did not have any significant bending moment observed.
h. Sliplining reduced the average strains in the steel pipes with 0% and 50% cutout but did not change the average strain in the steel pipe with 90% cutout. The unlined steel pipes with 0% and 50% cutout had significant bending moments developing around the springlines and the crown, respectively. Because of the arch effect of the unlined pipe with 90% cutout, no significant bending moment was observed in that pipe.

2. Field truck and plate loading tests on corroded steel pipes before and after sliplining:
   a. Grouting reduced the curvature at the invert of the liner.
   b. At 7 and 28 days after grouting, the average strains around the circumference of the liner decreased and the liner was fully under compression.
   c. At 7 days after grouting, positive bending happened at the springlines of the liner during grout hardening.
   d. In the truck loading tests, sliplining reduced the vertical diameter changes of the corroded steel pipe by approximately 78.2% and 81.5%, respectively, at 7 and 28 days after grouting.
   e. The applied wheel load on the top of the pipe induced a tensile strain on the inner face of the liner at the crown.
   f. In the plate loading tests, sliplining reduced the settlement of the pavement by 6% and 31%, respectively, at 7 and 28 days after grouting as compared with that before sliplining.
   g. In the plate loading tests, sliplining reduced the vertical diameter changes of the corroded steel pipes by 87% and 90%, respectively, at 7 and 28 days after grouting as compared with those before sliplining.

h. The applied pressure of 780 kPa on the loading plate induced a tensile strain around the liner and a negative curvature at both springlines at 7 days after grouting.

i. In both truck loading and plate loading tests at 7 and 28 days after grouting, loading only induced localized strain and curvature on the liner at the location of loading.

3. Footing loading tests on unlined and sliplined steel pipes with different degrees of corrosion in soil and parallel-plate loading tests of exhumed pipes in air:

   a. The models with the unlined pipes having 50% and 90% cutout had larger settlement than the model with the steel pipe having 0% cutout. Under the lower applied pressures, the model with the unlined pipe having 90% cutout had smaller settlement and vertical diameter changes than those having 50% cutout. The unlined steel pipe with 90% cutout had smaller horizontal diameter changes than the pipe with 50% cutout.

   b. The model with the sliplined steel pipe having a smaller percentage of cutout had a lower load capacity and higher footing settlement than that having a larger percentage of the cutout because the leaked grout made the bedding sand stronger under the pipe with a larger percentage of cutout stronger than that with a smaller percentage of cutout. Due to the arching behavior of the pipe with 90% cutout, the model with this pipe had higher stiffness than the steel pipe with 50% cutout. Under the lower applied pressures, the sliplined steel pipe with 90% cutout had higher stiffness than the unlined pipes with 50% and 90% cutout.

   c. The measured earth pressures induced by footing loading above the crown of the unlined pipe with 0% cutout were higher than those with 50% and 90% cutout.

   d. The measured vertical pressures under the invert and above the crown of the sliplined steel pipe with 0% cutout were approximately equal.

However, the measured vertical pressures above the crown of the sliplined steel pipes with 50% and 90% cutout were higher pressures than those under the invert.

e. The measured lateral pressures in the backfill with the unlined steel pipes having 0% cutout were higher than those having larger percentages of cutout. The measured lateral pressures at the level of the invert of the sliplined pipes were higher than those at the level of the springline.

f. In the parallel-plate loading tests on the exhumed pipes, the sliplined pipes with 50% and 90% cutout behaved stiffer than the sliplined pipe with 0% cutout. The vertical diameter changes of the sliplined pipes with 50% and 90% cutout were similar. Sliplining increased the load-carrying capacities of the unlined steel pipes.

6.2 Recommendations

This research investigated the effect of sliplining on the performance of corroded corrugated steel pipes under static loading. The following general recommendations can be made from this research:

1. Sliplining is an effective trenchless method for increasing the load capacity and stiffness of corroded steel pipes with the degree of corrosion at the invert up to 90%.
2. Sliplining reduces not only pipe deflection but also pavement settlement due to surface loading; therefore, it can be used to minimize pavements on corroded pipes from damaging.
3. Low-viscosity, high-strength grout is easier to fill the space between the corroded pipe and the liner under gravity and provides more load capacity, therefore, it should be used for sliplining instead of the FHWA low-strength grout.

Future research is needed to address the following issues:

1. Sliplining may reduce hydraulic capacity due to the reduction of the pipe cross-section; however, the plastic liner with a small roughness may increase hydraulic capacity. The impact of sliplining on hydraulic capacity was not addressed as a part of this study and may be a topic for future research.
2. The effects of the size and embedment depth of corroded pipes, the strength of grout, and the type and properties of liners on the performance of corroded steel pipes after sliplining should be investigated.
3. An analytical solution or design method for estimating the load-carrying capacity and deformation of the corroded steel pipes after sliplining is needed.
4. Future research should also evaluate the long-term performance of sliplined corroded steel pipes.

References

Acharya, R., Han, J., Brennan, J. J., Parsons, R. L., & Khatri, D. K. (2014). Structural response of a low-fill box culvert under static and traffic loading. *Journal of Performance of Constructed Facilities, 31*(1).

Ahmed, M. (2016). *Experimental investigations into the role of geosynthetic inclusions on the earth pressure acting on buried structures* (Doctoral dissertation). McGill University, Montreal, Quebec.

Al-Naddaf, M., Han, J., Xu, C., & Rahmaninezhad, S. M. (2018). Effect of geofoam on vertical stress distribution on buried structures subjected to static and cyclic footing loads. *Journal of Pipeline Systems Engineering and Practice, 10*(1).

American Association of State Highway and Transportation Officials (AASHTO). (2009). *AASHTO LRFD bridge construction specification* (2nd ed.). Washington, D.C.: Author.

ASTM C39 / C39M-04. (2004). *Standard test method for compressive strength of cylindrical concrete specimens*. West Conshohocken, PA: ASTM International. doi: 10.1520/C0039_C0039M-04, www.astm.org.

ASTM D1195 / D1195M-09. (2015). *Standard test method for repetitive static plate load tests of soils and flexible pavement components, for use in evaluation and design of airport and highway pavements*. West Conshohocken, PA: ASTM International. doi: 10.1520/D1195_D1195M-09R15, www.astm.org

ASTM D2412-11. (2018). *Standard test method for determination of external loading characteristics of plastic pipe by parallel-plate loading*. West Conshohocken, PA: ASTM International. doi: 10.1520/D2412-11R18, www.astm.org

ASTM D3080 / D3080M-11. (2011). *Standard test method for direct shear test of soils under consolidated drained conditions*. West Conshohocken, PA: ASTM International. doi: 10.1520/D3080_D3080M-11, www.astm.org

ASTM D6951 / D6951M-18. (2018). *Standard test method for use of the dynamic cone penetrometer in shallow pavement applications*. West Conshohocken, PA: ASTM International. doi: 10.1520/D6951_D6951M-18, www.astm.org

Ballinger, C. A., & Drake, P. G. (1995). *Culvert repair practices manual: Volume I* (Report No. FHWA-RD-94-096). McLean, VA: Federal Highway Administration.

Bloomquist, D., Boyd, A., Chen, Y., & Crosby, M. (2009). *Load response comparison between fiber and steel reinforced concrete pipe – Phase two*. Tallahassee, FL: Florida Department of Transportation.

Han, J., Acharya, R., Parsons, R. L., & Khatri, D. (2013). *Improved load distribution for load rating of low-fill box structures* (Report No. K-TRAN: KU-12-3). Topeka, KS: Kansas Department of Transportation.

Han, J., Rahmaninezhad, S. M., Parsons, R. L., & Wang, F. (2018). *Software for load distribution on low-fill box culverts: User's manual* (Report No. K-TRAN: KU-16-5). Topeka, KS: Kansas Department of Transportation.

Han, J., Wang, F., Khatri, D. K., & Parsons, R. L. (2015). *Establishing a design procedure for buried steel-reinforced high-density polyethylene pipes: A field study* (Report No. K-TRAN: KU-14-4). Topeka, KS: Kansas Department of Transportation.

Hong, W. P., Hong, S., & Kang, T. H.-K. (2016). Lateral earth pressure on a pipe buried in soft grounds undergoing lateral movement. *Journal of Structural Integrity and Maintenance, 1*(3), 124–130.

Kakrasul, J. I., Han, J., Rahmaninezhad, S. M., & Weldu, M. (2016). Model tests of geosynthetic-reinforced earth walls with limited-space retained fill. In *GeoAmericas 2016 Proceedings* (Vol. 1, pp. 1279–1286). Jupiter, FL: Minerva Technology, Resources, & Information.

Khatri, D. K., Han, J., Corey, R., Parsons, R. L., & Brennan, J. J. (2015). Laboratory evaluation of installation of a steel-reinforced high-density polyethylene pipe in soil. *Tunnelling and Underground Space Technology*, *49*, 199-207.

Khatri, D. K., Han, J., Parsons, R. L., Young, B., Brennan, J. J., & Corey, R. (2013). Laboratory evaluation of deformations of steel-reinforced high-density polyethylene pipes under static loads. *Journal of Materials in Civil Engineering, 25*(12), 1964–1969.

Machelski, C., Michalski, J. B., & Janusz, L. (2009). Deformation factors of buried corrugated structures. *Transportation Research Record, 2116*, 70–75.

Mahgoub, A., & El Naggar, H. (2018). Using TDA as an engineered stress-reduction fill over preexisting buried pipes. *Journal of Pipeline Systems Engineering and Practice, 10*(1).

Mai, V. T. (2013). *Assessment of deteriorated corrugated steel culverts* (Master's thesis). Queen's University, Kingston, Ontario.

Mai, V. T., Hoult, N. A., & Moore, I. D. (2013). Effect of deterioration on the performance of corrugated steel culverts. *Journal of Geotechnical and Geoenvironmental Engineering, 140*(2).

Simpson, B., Hoult, N. A., & Moore, I. D. (2017). Rehabilitated reinforced concrete culvert performance under surface loading. *Tunnelling and Underground Space Technology, 69*, 52–63.

Simpson, B., Moore, I. D., & Hoult, N. A. (2015). Experimental investigation of rehabilitated steel culvert performance under static surface loading. *Journal of Geotechnical and Geoenvironmental Engineering, 142*(2).

Smith, T., Hoult, N. A., & Moore, I. D. (2015). Role of grout strength and liners on the performance of slip-lined pipes. *Journal of Pipeline Systems Engineering and Practice, 6*(4).

Rahmaninezhad, S.M., Han, J., Al-Naddaf, M., and Parsons, R.L. (2019). Behavior of sliplined corrugated steel pipes under parallel-plate loading. *Journal of Materials in Civil Engineering, 31*(10).

Rahmaninezhad, S. M., Yasrobi, S. S., & Eftekharzadeh, S. F. (2009). Effects of compaction in the subgrade of the reinforced sand backfills with geotextile on bearing capacity. *International Journal of Civil Engineering, 12*, 320–328.

Regier, C. E. (2015). *Investigation of the failure mechanisms of intact and deteriorated culverts* (Master's thesis). Queen's University, Kingston, Ontario.

Tetreault, J. (2016). *Performance and assessment of rehabilitated steel culverts* (Master's thesis). Queen's University, Kingston, Ontario, Canada.

Wang, F., Han, J., Khatri, D. K., Parsons, R. L., Brennan, J. J., & Guo, J. (2015). Field installation effect on steel-reinforced high-density polyethylene pipes. *Journal of Pipeline Systems Engineering and Practice, 7*(1).

Zarnani, S., El-Emam, M. M., & Bathurst, R. J. (2011). Comparison of numerical and analytical solutions for reinforced soil wall shaking table tests. *Geomechanics and Engineering, 3*(4), 291–321.

K-TRAN

KANSAS TRANSPORTATION RESEARCH AND NEW-DEVELOPMENT PROGRAM

AD ASTRA PER ASPERA

Kansas

Department of Transportation